

Injection of enriched lithospheric mantle magmas explains the formation of microgranular enclaves in the Rio Jacaré Batholith, Borborema Province, Brazil

Carlos Santana Sousa^{1,2*} , Hiakan Santos Soares^{1,2} , Maria de Lourdes da Silva Rosa^{2,3} ,
Herbet Conceição^{1,2,3} 

Abstract

The Rio Jacaré Batholith (RJB; 617 ± 4 Ma) is inserted in the Poço Redondo Domain, Sergipano Orogenic System. This batholith is formed by monzodiorite, quartz monzodiorite, monzonite, and quartz monzonite, with abundant microgranular enclaves (MEs). The MEs vary from black to light gray and exhibit globular to slightly elongated shapes with clear-cut, crenulated, and cusped, or, more rarely, diffuse contacts. They correspond to diorites, monzodiorites, quartz monzodiorites, and monzonites, and textural features indicate mixing of magmas, such as compositional zoning in plagioclase, inclusion zones in plagioclase phenocrysts, poikilitic alkali feldspar, acicular apatite, and ocellar quartz. Calculations of linear correlations of major elements showed that the smallest fraction of mafic magma involved in the mixing was 0.43. MEs represent the breakdown and cooling of a mafic magma that was injected into a cooler felsic magmatic chamber. Emplacement of this mafic magma occurred at different stages of crystallization of the RJB magmatic chamber. The MEs are magnesian and metaluminous, with affinity to the shoshonitic series. Ratios for Ba/Nb (> 23), Ba/La (> 15), and Nb/La (0.22–0.69) are characteristic of magmas generated from partial melting of an enriched lithospheric mantle source. Batch melting modeling suggests that source melting rates of less than 3% are necessary to generate magmas similar to those of the RJB MEs.

KEYWORDS: Sergipano orogenic system; mixing; mingling; shoshonitic magmatism.

INTRODUCTION

According to Elburg (1996), there are four types of enclaves formed by different processes:

- restite is a solid residue resulting from magma generation (e.g., Chen *et al.* 1990);
- xenoliths are fragments of country rock (e.g., Hall 1991);
- enclaves are formed through the segregation of early mafic minerals (e.g., Dodge and Kistler 1990);
- microgranular enclaves (MEs) are cooled droplets of mafic magmas that intruded host granitic magmas (e.g., Didier 1973, Clemens *et al.* 2017, Siuda and Bagiński 2019).

MEs are the most common types of inclusions in granitic bodies (Barbarin and Didier 1991) and are considered to be one

of the keys to understanding the genesis and evolution of granites (Didier 1973, Barbarin and Didier 1991, Sarjoughian *et al.* 2017).

Some authors consider the presence of MEs with cooled edges and xenocrysts in granites as evidence of the coexistence of magmas with different viscosities (e.g., Vernon 1984, Kumar and Rino 2006, Siuda and Bagiński 2019). The rocks formed have characteristic textures (e.g., rapakivi texture, ocellar quartz, inclusion zones in phenocrysts, compositional zoning in plagioclase, and biotite blades) that indicate the actions of mingling between magmas (Hibbard 1991). Geochemical data can also preserve evidence of mixing; the mixing can cause, for example, the predominance of intermediate compositions, resulting from the mixture of basic and acid magmas, and linear trends in Harker-type diagrams (e.g., Nardi and Lima 2000, Reubi and Blundy 2009, Ruprecht *et al.* 2012, Kumar *et al.* 2017).

In the Sergipano Orogenic System (SOS; Conceição *et al.* 2016), there is evidence of voluminous Neoproterozoic plutonism that has been the target of several studies over the last few decades (e.g., Santos and Souza 1988, Davison and Santos 1989, Santos *et al.* 2001, Bueno *et al.* 2009, Oliveira 2014, Oliveira *et al.* 2015, Conceição *et al.* 2016, Fontes *et al.* 2018, Lisboa *et al.* 2019, Pinho Neto *et al.* 2019, Santos *et al.* 2019, Sousa *et al.* 2019, Fernandes *et al.* 2020). Many of these studies identified the presence of MEs in these intrusions; however geological, petrographic, and geochemical data from MEs in the SOS are still scarce.

¹Programa de Pós-Graduação em Geologia, Instituto de Geociências, Universidade Federal da Bahia – Salvador (BA), Brazil. E-mails: karlcss@ufba.br, hiakanss@ufba.br, herbet@academico.ufs.br

²Laboratório de Petrologia Aplicada à Pesquisa Mineral, Universidade Federal de Sergipe – São Cristóvão (SE), Brazil. E-mail: lrosa@academico.ufs.br

³Programa de Pós-Graduação em Geociências e Análise de Bacias, Universidade Federal de Sergipe – São Cristóvão (SE), Brasil.

*Corresponding author.



This study presents and discusses the geological, petrographic, and geochemical data of the MEs of the Rio Jacaré Batholith (RJB), which is an important intrusion in the Poço Redondo Domain (PRD), located in the northern sector of the SOS.

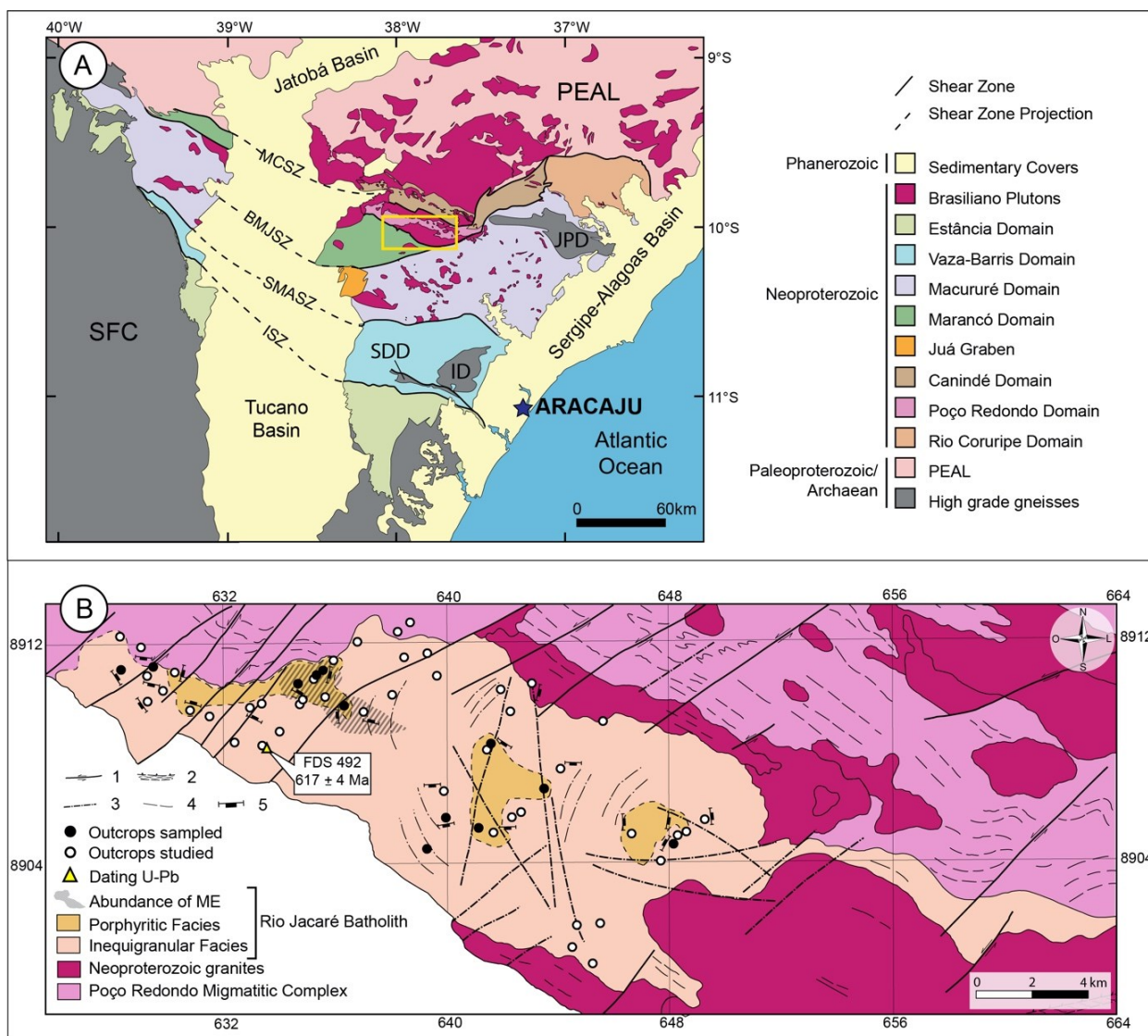
REGIONAL CONTEXT

The SOS (Fig. 1A) is inserted in the southern portion of the Borborema Province (Almeida *et al.* 1977). This orogen is interpreted to be the result of the collision between the Sanfranciscana plate, to the south, and the Pernambuco-Alagoas Domain, to the northeast, during the Brasiliano Orogeny (D'el Rey Silva 1992, Oliveira *et al.* 2006, 2010). The seven geological domains of the SOS are limited by shear zones (Davison and Santos 1989, Silva Filho and Torres 2002): Estância, Vaza-Barris, Macururé, Maracó, Poço Redondo, Canindé, and Rio Coruripe. The Macururé, Maracó, Poço Redondo, and Canindé domains are characterized by abundant presence of granites.

The RJB occurs in the PRD (Fig. 1B), which, according to Santos *et al.* (2001), represents the deepest crustal exposure of the SOS. This domain is formed by the Poço Redondo Migmatitic Complex (Santos and Souza 1988) and by Neoproterozoic granites (Carvalho 2005, Pinho Neto *et al.* 2019, Sousa *et al.* 2019). The PRD is limited to the north by the Canindé Domain and the Macururé Shear Zone (Fig. 1A) and to the south by the Maracó Domain and the Poço Redondo Shear Zone.

Microgranular enclaves in the Sergipano Orogenic System

In the SOS, MEs have been described in several intrusions (Table 1). These enclaves, according to several authors (e.g., Gentil 2013, Silva 2014, Lima 2016, Lisboa *et al.* 2019, Pereira *et al.* 2019, Santos *et al.* 2019, Fernandes *et al.* 2020), show globular and elliptical shapes. Their sizes range from centimetric to metric.



1: Fault; 2: Shear zone; 3: Fracture; 4: Lineament; 5: Magmatic foliation.

Figure 1. Geological schemes that contextualize the regional and local geology of the Rio Jacaré Batholith. (A) Sergipano Orogenic System (Oliveira *et al.* 2006, after Pinho Neto *et al.* 2019); (B) Rio Jacaré Batholith (Sousa *et al.* 2019). São Francisco Craton (SFC); Pernambuco-Alagoas Massif (PEAL). Shear zones: Macururé (MCSZ); Belo Monte Jeremoabo (MBJSZ); São Miguel do Aleixo (SMASZ); Itaporanga (ISZ). Domes: Itabaiana (ID); Simão Dias (SDD); and Jirau do Ponciano (JPD).

In the granites of the Macururé and Poço Redondo domains (e.g., Oliveira 2014, Silva 2014, Lisboa *et al.* 2019, Sousa *et al.* 2019, Fernandes *et al.* 2020), multiple enclaves, some with chilled margins, are described. These enclaves are randomly distributed in the intrusions or gathered in syn-plutonic dikes. In several of these enclaves, alkaline feldspar xenocrystals attributed to the host granites occur. These features provide evidence for mixing between mafic and felsic magmas during the evolution of these intrusions (e.g., Lisboa *et al.* 2019, Sousa *et al.* 2019).

The MEs of the Ediacaran bodies in the SOS have compositions ranging from diorite, quartz diorite, monzodiorite, quartz monzodiorite, monzonite, syenite, and alkali-feldspar syenite to alkali-feldspar-quartz syenite (Fig. 2A). The mafic minerals in these rocks are hornblende, biotite, diopside, and titanite, as accessory minerals, magmatic epidote, apatite, opaque minerals, and zircon are found. These rocks have silica contents varying from 44% to 63%, pointing to distinct degrees of evolution (Fig. 2B), and they have an affinity with shoshonitic series (Fig. 2C).

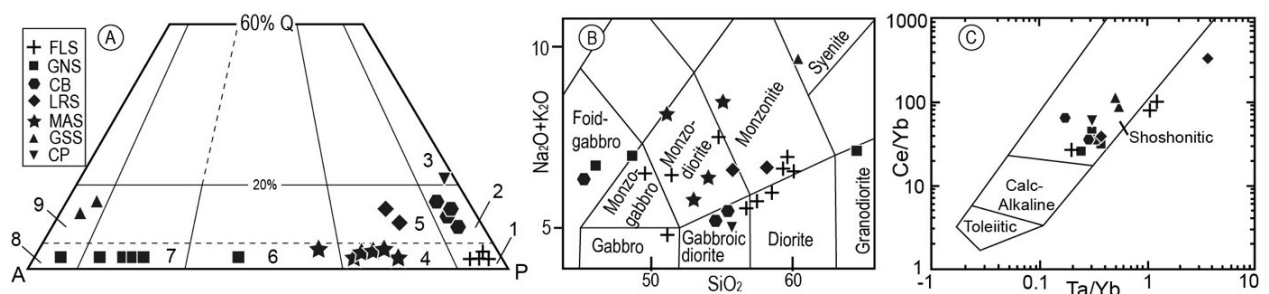
Rio Jacaré Batholith

The RJB (167 km²) has a U-Pb_{SHRIMP} zircon crystallization age of 617 ± 4 Ma (Sousa *et al.* 2019). It is intrusive to the Poço Redondo Migmatitic Complex and Sítios Novos Batholith (Sousa *et al.* 2019). This batholith is composed of monzodiorite, quartz monzodiorite, monzonite, and quartz monzonite, which occur in two petrographic facies, inequigranular, and porphyritic (Fig. 1); they always present abundant MEs.

The Inequigranular Facies (Fig. 3A) is predominant in the RJB and consists of gray rocks with a medium to fine inequigranular texture. Eventually, these rocks have magmatic foliation and the elongated enclaves appear parallel or subparallel to the foliation of the host rocks. The Porphyritic Facies (Fig. 3B) differs from the previous facies due to the presence of alkali feldspar phenocrysts to macrocrystals, with sizes ranging from 1 to 5 cm. The rocks of these facies are composed of plagioclase (An₁₁₋₃₃), microcline (Or₇₅₋₉₈), quartz, biotite (0.3 < Fe/(Fe + Mg) < 0.6), Mg-hornblende, titanite, magmatic epidote, F-apatite, magnetite, ilmenite, and zircon.

Table 1. Characteristics of the host plutons of MEs in the Macururé and Poço Redondo Domains of the Sergipano Orogenic System.

Pluton	Location	Rocks	Geochemistry affinity	Crystallization age (U-Pb _{SHRIMP})	Reference
Curitiba Batholith	Poço Redondo Domain	Monzogranite, syenogranite, monzonite, and syenite	Shoshonitic	624 ± 16 Ma	Gentil (2013), Lima (2016)
Capela Stock	Macururé Domain	Diorite, hornblendite, gabbro, and granite	Shoshonitic	631 ± 3 Ma	Pereira <i>et al.</i> (2019)
Glória Sul Stock	Macururé Domain	Syenogranite	High K calc-alkaline	626 ± 7 Ma	Conceição <i>et al.</i> (2016), Rosa <i>et al.</i> (2017)
Fazenda Lagoas Stock	Macururé Domain	Granodiorite, granite, and quartz monzonite	Shoshonitic	623 ± 4 Ma	Fernandes <i>et al.</i> (2020)
Monte Alegre Stock	Macururé Domain	Monzonite and granite	High K calc-alkaline	621 ± 5 Ma	Oliveira (2014), Rosa <i>et al.</i> (2017)
Lagoa do Roçado Stock	Macururé Domain	Granodiorite	High K calc-alkaline	618 ± 4 Ma	Silva (2014)
Propriá Stock	Macururé Domain	Monzonite and Granite	High K calc-alkaline	615 ± 6 Ma	Santos <i>et al.</i> (2019)
Glória Norte Stock	Macururé Domain	Quartz monzonite and monzogranite	Shoshonitic	588 ± 5 Ma	Lisboa <i>et al.</i> (2019)



Q: quartz; A: alkali feldspar + albite with < 5% anorthite; P: plagioclase (anorthite > 5%); 1: Diorite; 2: quartz diorite; 3: tonalite; 4: monzodiorite; 5: quartz monzodiorite; 6: monzonite; 7: syenite; 8: alkali-feldspar syenite; 9: alkali-feldspar-quartz syenite. GNS: Glória Norte Stock (Lisboa *et al.* 2019); CB: Curitiba Batholith (Gentil 2013); LRS: Lagoa do Roçado Stock (Silva 2014); MAS: Monte Alegre Stock (Oliveira 2014); GSS: Glória Sul Stock (Conceição *et al.* 2016); CP: Capela Pluton (Pereira *et al.* 2019); FLS: Fazenda Lagoas Stock (Fernandes *et al.* 2020).

Figure 2. Modal and chemical diagrams applied to the enclaves of different bodies of the geological domains of the SOS. (A) Streckeisen's (1976) QAPF triangular diagram. (B) TAS diagram with fields proposed by Middlemost (1985). (C) Ta/Yb versus Ce/Yb diagram with fields defined by Pearce (1982).

The RJB rocks are magnesian and metaluminous, and have a high-K calc-alkaline affinity and geochemical signature consistent with a post-collisional environment (Brito 1996, Sousa *et al.* 2019).

According to Oliveira *et al.* (2015), the RJB was probably formed by a mixture of mantle-derived and crustal magmas. These authors support this hypothesis based on $(^{87}\text{Sr}/^{86}\text{Sr})_i$ ratios ranging from 0.70656 to 0.70789, with $\epsilon_{\text{Nd}(617\text{Ma})}$ between -1.15 and -2.55 and T_{DM} ranging from 1.2 to 1.3 Ga.

MATERIALS AND METHODS

The studied samples correspond to MEs, with colors ranging from light gray to dark gray. These rocks show no evidence of alteration and have magmatic textures. In this study, only samples from the central parts of the enclaves were collected in an attempt to avoid possible interactions between the periphery and the host magma. After grinding, the feldspar xenocrysts present in some enclaves were manually removed in order to obtain chemical data that corresponded as close as possible to the composition of the original magma that originated these rocks.

In this study, rocks were named using the International Union of Geological Sciences recommendations (Le Maitre *et al.* 1989), and the modal data were obtained from the modified CIPW standard norm for hornblende-bearing rocks.

The geochemical analysis of major elements was obtained from pressed pellets using a Shimadzu XRF-1800 x-ray fluorescence spectrometer at the Condominium of Multiuser Laboratories of Geosciences of the Federal University of Sergipe. The pellets were made by mixing the samples with boric acid, which was sprayed onto the samples, with a ratio of samples to boric acid of 3:1. Then, the sample/boric acid mixtures were pressed in a hydraulic press with a pressure of 60 kN for 30 s. The degree of confidence of the analysis was evaluated through a comparison with certified reference materials (e.g., AVG-1, DTS-1, and QLO-1). The loss of ignition was determined by calcinating the samples at a constant temperature of 1,000°C in a muffle furnace for 2 h.

The trace elements were performed at the ALS commercial laboratory (details can be obtained on the lab website — www.alsglobal.com), Canada, through the package ME-MS81D. The method consists of lithium borate fusion prior to acid dissolution and ICP-MS analysis.

MICROGRANULAR ENCLAVES OF THE RIO JACARÉ BATHOLITH

Geology

The RJB MEs are fine-grained and show sizes from 2 cm to 2 m, black to light gray colors, globular to elliptical shapes, and clear-cut, crenulated, and diffuse types of contacts.

In the eastern portion of the RJB, the MEs have smaller sizes, round shapes (Fig. 4A), and black color, and they are isolated. In the western region, the MEs are more abundant, have larger sizes, and occur more frequently in syn-plutonic dikes (Figs. 4B-4D). These dikes are subvertical and have widths ranging from 1.5 to 6 m, and their lengths are greater than 10 m. In the western sector, there is a greater variety of enclave shapes exhibiting rounded to elongated features. They tend to present varying shades of gray.

Globular to elongated MEs with clear-cut contacts (Fig. 4E) predominate throughout the RJB. The elongated types are oriented parallel to the batholith's magmatic foliation. In the western region, the MEs are also clear-cut but with more complex contacts (Fig. 4F), including crenulated (Fig. 4G), lobate, sinuous, and cusped. The MEs with crenulated contacts are typically 15 cm long, while the MEs with other types of contacts are larger.

Some MEs have a grain size that decreases from the nucleus to the border (Fig. 4E). Alkali feldspar and quartz xenocrysts in the MEs are recurrent features and can be identified by their grain size, which is similar to that of the host granite and larger than the grain size of the MEs (Fig. 4H). In some cases, multiple MEs are observed in the center of the RJB (Fig. 4I); these enclaves are gray and contain smaller, black enclaves. These black enclaves occur both within the gray enclaves and in the host granite.



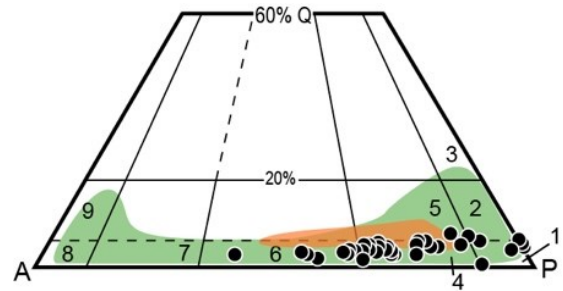
Figure 3. RJB rocks in the field. (A) Inequigranular Facies and (B) Porphyritic Facies. Note the centimetric sizes of the alkali feldspar crystals and the finer grain of the matrix. Pinkish minerals with rectangular sections correspond to alkali feldspar crystals, white minerals correspond to plagioclase, and black minerals correspond to biotite and hornblende. The diameter of the black circle is 7 cm.

Petrography

The RJB MEs have dioritic, monzodioritic, quartz monzodioritic, and monzonitic compositions (Fig. 5). These rocks are composed essentially of plagioclase (An_{11-51} ; 37–64% in volume), microcline (1–15%), quartz (2–17%), hornblende (3–26%), and biotite (8–33%). The accessory minerals are titanite, epidote, allanite, F-apatite, magnetite, ilmenite, and zircon. MEs have a massif structure with fine-grained, porphyritic, and hypidiomorphic textures (Fig. 6A). In the porphyritic rocks, there are plagioclase phenocrysts and microcline and ocellar quartz xenocrysts (Figs. 6B and 6C). All the textures observed in these rocks are igneous and show no evidence of solid-state deformation or recrystallization.

Plagioclase occurs as phenocrysts (1.7–5.8 mm) and in the matrix (0.1–1.4 mm). These crystals are subhedral and show albite and albite-Carlsbad twinning and frequent compositional zoning. The zoning is parallel to the crystal faces and marked by the presence of opaque, biotite, and hornblende mineral inclusions (Fig. 6D). In some crystals, zoning develops from rounded plagioclase nuclei, suggesting

dissolution (Fig. 6E). Patchy, boxy, cellular, and stepwise textures can occasionally occur, indicating complex evolution during crystallization. Sometimes, saussuritization is



Q: quartz; A: alkali feldspar + albite with < 5% anorthite; P: plagioclase (anorthite > 5%). 1: Diorite; 2: quartz diorite; 3: tonalite; 4: monzodiorite; 5: quartz monzodiorite; 6: monzonite; 7: syenite; 8: alkali-feldspar syenite; 9: alkali-feldspar-quartz syenite.

Figure 5. Classification of the RJB MEs using the QAP diagram (Streckeisen 1976). The orange area represents the composition of the RJB rocks. The green area represents the compositions of the other SOS MEs.



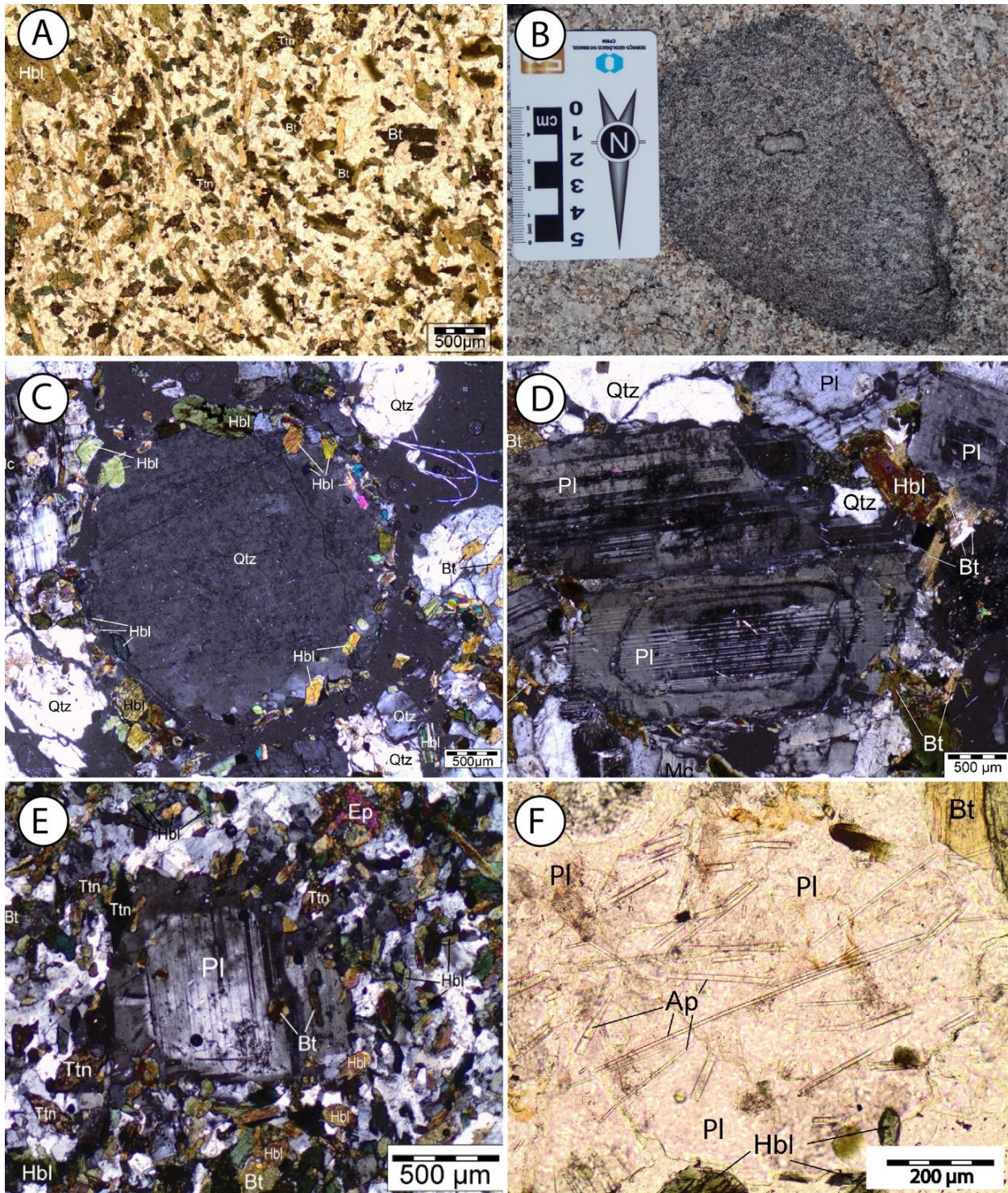
Figure 4. Field images showing different structures of the various types of MEs identified in the RJB. (A) MEs with globular to elongated shapes and clear-cut straight contacts. (B, C, and D) Set of elongated enclaves with different sizes interpreted as syn-plutonic dikes. Note the feature in the left corner of image D suggesting that the enclave's magma was undergoing rupture as it generated MEs. (E) ME with clear-cut contacts, showing a grain size increase from the edges to the center. Note the darker edges. (F) ME with crenulated to lobate margins. (G) Round ME with a crenulated contact in its left portion. (H) Alkali feldspar xenocrysts in ME. It is possible to observe crystals penetrating the enclave edges. (I) Multiple MEs in the RJB. Note the black enclaves inside the larger gray enclave.

observed in the grain nuclei of some crystals. A myrmekitic texture is occasionally present.

Perthitic microcline is anhedral, poikilitic, and occurs in the matrix (0.1–1.5 mm) and as xenocrysts (1.7–11.7 mm). It often shows albite-pericline twinning, but occasionally remnants of Carlsbad twinning are found. Quartz presents a weak undulose extinction. It occurs in the matrix (0.1–1.3 mm) and sometimes as xenocrysts (1.5–4.3 mm) in the ocellar texture

(Figs. 6B and 6C), which shows zones of biotite and hornblende inclusion at the edges.

Brown biotite is subhedral and has brown to yellow pleochroism. It is frequently associated with hornblende crystals in mafic aggregates. Titanite crystals and anhedral opaque minerals occur as inclusions in grain margins and in cleavage planes. Green hornblende is subhedral to euhedral and presents pleochroism in shades of green. It



Qtz: quartz; Hbl: hornblende; Bt: biotite; Pl: plagioclase; Ttn: titanite; Ep: epidote; Ap: apatite.

Figure 6. RJB ME textures. (A) General view of the ME texture (parallel nicols). (B) Macroscopic image of ME showing the quartz ocellar texture (note black minerals at the edges of the crystal). (C) Quartz with ocellar texture. Note hornblende inclusions only at the edges of the crystal. (D) Compositional zoning and inclusion zone in plagioclase. Note that the compositional zoning and the inclusion zone are parallel to each other. (E) Plagioclase showing a nucleus with rounded faces and compositional zoning at the edges. (F) Acicular apatite crystals.

commonly occurs in clusters along with biotite, titanite, and opaque minerals.

Epidote is subhedral or anhedral. Anhedral crystals are usually observed in the contacts with biotite, hornblende, and plagioclase. The subhedral crystals are considered to be magmatic, showing dissolution features. They can also occur as rims around allanite crystals. Rarely, vermicular quartz inclusions are observed in the epidote. Allanite occurs sporadically and subhedral titanite occurs as inclusions in most minerals and locally formed clusters. Apatite is euhedral and acicular (Fig. 6F), and, as individual elongated grains, it may be found often included in various minerals (e.g., in plagioclase and biotite). Zircon is euhedral (~0.1 mm) and occurs as inclusion. Anhedral opaque minerals (magnetite and ilmenite) no larger than 0.4 mm are associated with biotite, hornblende, and titanite crystals.

Geochemistry

The chemical data of representative samples of the RJB MEs are shown in Tables 2 and 3.

In the $\text{Na}_2\text{O} + \text{K}_2\text{O}$ versus SiO_2 diagram, MEs are placed in the monzogabbro, monzodiorite, monzonite, and quartz monzonite fields (Fig. 7A). Most samples show SiO_2 contents of 53–61 wt%, except for sample SOS-850B, which has 48% SiO_2 . The MgO (2.5–7.17%), K_2O (2.05–7.54%), Fe_2O_3 (5.5–12.21%), CaO (3.5–8.21%), and Na_2O (2.1–4.63%) contents of the MEs also show wide variation. The Al_2O_3 content varies little (13.61–16.69%). The total amount of alkalis ($\text{Na}_2\text{O} + \text{K}_2\text{O}$) in the studied rocks ranges from 5.87% to 9.64%, and the $\text{K}_2\text{O}/\text{Na}_2\text{O}$ ratio ranges from 0.46 to 3.59.

The RJB MEs are metaluminous (Fig. 7B) and belong to the magnesian suite (Fig. 7C). The $\text{K}_2\text{O}-\text{SiO}_2$, $\text{K}_2\text{O}-\text{Na}_2\text{O}$, and $\text{Ce}/\text{Yb}-\text{Ta}/\text{Yb}$ relationships indicate a shoshonitic affinity (Figs. 8A–8C). There is an increase in K_2O in a group of samples with SiO_2 contents between 58 and 61%, splitting the population into two groups: one is positioned in the calc-alkaline field and the other in the shoshonitic field (Fig. 8A). This K_2O variation may be due to an increase in the volume of alkali feldspar. The rare earth element patterns (Fig. 9) show enrichment in light rare earth elements (LREEs) rather than in heavy rare earth elements (HREEs). The $[\text{La}/\text{Yb}]_N$ and $[\text{La}/\text{Sm}]_N$ ratios range from 9.08 to 33.26 and from 2.04 to 4.77, respectively. Negative Eu anomalies are present with Eu/Eu^* ranging from 0.48 to 0.88. It is observed that the samples are distributed into three groups of spectra (Fig. 9): 1: the sample SOS 850B (48.09% SiO_2), which has a higher sum of ETR; 2: a set of samples with weak negative Eu anomalies (0.68–0.88); and 3: samples SOS 844B and SOS 867B, which show the most negative Eu anomalies (0.48–0.65).

DISCUSSION

The MEs found in the RJB are easily observed in the field due to their abundance, high frequency in outcrops, and dark color, and because they are fine-grained, differing from the light-colored rocks that dominate this batholith. According

to Kumar *et al.* (2004), enclaves with grain sizes finer than the host granites and lacking cumulate texture are not the residuum of a fractional crystallization that might have generated the host. According to Torkian and Furman (2015), the presence of MEs with fine-grained margins, microgranular or/and porphyritic textures, plagioclase crystals showing disequilibrium textures, and compositional variation indicates that these enclaves are products of magmatic mingling. These features are found in the RJB MEs and suggest that they were formed from magma and do not represent cumulates or restites. Therefore, the nature of these enclaves must reflect magmatic processes, such as the mixing of magmas and fractional crystallization.

Evidence for mixing and mingling processes

Mixing

The RJB MEs show a large variation in their SiO_2 content (48–61%), but intermediate compositions predominate. According to Reubi and Blundy (2009) and Ruprecht *et al.* (2012), the generation of rocks with intermediate compositions results, in most cases, from the coexistence and mixing of contrasting magmas. According to Janoušek *et al.* (2004), the compositional variation of MEs can be considered the mixing of a mantle-derived mafic magma with crustal magmas. Some authors (e.g., Barbarin and Didier 1991, Shukla and Mohan 2019) consider some features that are also found in the RJB MEs (e.g., variation in the color of the MEs, presence of multiple MEs, and diffuse contacts), a reflection of different degrees of homogenization and the role of mixing between the parental mafic magma and the felsic host.

The mixing of two magmas only occurs when their viscosities are similar (Fernandez and Barbarin 1991, Weidendorfer *et al.* 2014). According to Winter (2014), the catazone is a region in the crust where rocks experience high temperatures and the viscosity difference between different materials is relatively low. According to Sousa *et al.* (2019), the RJB rocks, the host rocks of the studied MEs, were crystallized at a depth of 25 km with a Mg-hornblende crystallization temperature of 826°C. Probably, these emplacement conditions of the RJB allowed its magma and the ME magma to have similar viscosities, favoring mixing processes to occur.

Mixing between magmas can often be inferred by identifying linear trends in binary diagrams. The samples studied in the CaO/SiO_2 versus $\text{FeO}_t/\text{SiO}_2$ diagram show an alignment that suggests that mixing between magmas has occurred (Fig. 10A). This trend is consistent with two mixing components: a mafic magma (enclaves) and a felsic magma (host granite).

The variation in the SiO_2 content of the RJB MEs suggests that the compositions represent different degrees of hybridization. Therefore, the relative contributions of the mafic and felsic magmas were estimated using the linear correlation of major elements with the mixing algorithm of Fourcade and Allegre (1981). According to these authors, if mixing occurs, this process will affect each chemical element of the magmas, so that it will satisfy the following relation (Eq. 1):

Table 2. Chemical analysis of major and minor elements and normative compositions (CIPW standard with hornblende) of the RJB MEs.

%	SOS 850B	SOS 876B	SOS 867B	SOS 860E	SOS 853B	SOS 849B	SOS 861B	SOS 871B	SOS 861S	SOS 844B	SOS 861M	SOS 853D	SOS 861L	SOS 853I	SOS 861O	SOS 853C	SOS 853G	SOS 861Q	SOS 861P	SOS 860D
SiO ₂	48.09	53.99	55.04	55.39	55.52	55.55	55.88	56.56	56.86	57.23	58.19	58.33	58.34	58.49	58.62	58.63	58.65	58.72	58.72	58.74
TiO ₂	1.92	1.29	0.82	0.88	0.56	1.34	0.54	0.61	0.65	0.83	0.72	1.04	0.69	1.35	0.69	0.89	0.92	0.70	0.71	0.73
Al ₂ O ₃	16.69	15.23	15.08	15.49	14.04	15.13	13.83	13.61	14.19	14.35	15.01	15.16	15.50	16.51	15.22	15.82	16.13	14.85	15.08	15.15
Fe ₂ O ₃	12.22	9.74	8.61	8.56	8.80	8.99	8.16	9.55	7.00	8.59	6.97	7.27	6.14	5.50	6.92	5.80	5.98	6.77	6.78	6.67
MnO	0.14	0.12	0.12	0.10	0.14	0.14	0.15	0.13	0.13	0.18	0.10	0.11	0.08	0.08	0.09	0.07	0.06	0.10	0.10	0.08
MgO	5.22	5.82	4.80	5.05	7.17	4.77	4.50	6.84	4.89	5.83	2.96	4.02	2.64	2.59	3.35	2.53	2.71	3.08	3.06	3.56
CaO	8.22	7.06	6.04	5.30	6.71	6.17	5.97	5.78	5.50	5.37	5.22	5.25	4.70	3.96	4.76	3.93	3.73	4.99	4.95	4.69
Na ₂ O	3.59	3.60	3.79	3.93	3.55	4.57	2.10	2.73	2.74	3.63	3.69	4.05	3.65	4.64	4.03	4.46	4.34	3.65	3.74	3.84
K ₂ O	2.99	2.28	4.07	4.38	2.63	2.15	7.54	3.69	6.27	3.03	5.14	3.27	5.88	4.20	4.34	4.92	4.60	5.16	4.85	4.26
P ₂ O ₅	1.08	0.55	0.70	0.85	0.33	0.37	0.67	0.25	0.72	0.36	0.74	0.62	0.79	1.16	0.67	1.14	1.03	0.71	0.71	0.66
LOI	0.31	0.77	0.72	0.87	0.86	0.62	0.66	0.93	0.76	0.48	0.71	0.59	0.88	0.84	0.60	0.63	0.83	0.88	0.93	0.73
Total	100.46	100.45	99.79	99.81	100.32	99.80	100.00	100.69	99.71	99.88	99.45	99.70	99.29	99.32	99.29	98.80	98.97	99.62	99.62	99.3
Q	4.05	13.52	9.32	8.76	14.15	11.54	8.04	17.69	10.36	16.27	10.53	14.60	8.84	10.27	12.11	9.40	10.91	11.47	11.97	13.24
Or	5.64	0.09	12.97	16.59		1.72	34.22	6.05	25.77	4.46	23.53	10.05	28.65	18.86	17.92	23.23	20.98	23.40	21.59	16.95
Ab	30.38	30.44	32.08	33.27	30.07	38.67	17.77	23.10	23.19	30.74	31.24	34.26	30.92	39.25	34.13	37.74	36.68	30.89	31.61	32.50
An	20.60	18.66	12.12	11.68	14.58	14.42	6.04	13.99	7.91	13.90	9.22	13.54	8.55	11.82	10.60	8.61	10.95	8.90	10.06	11.51
Wo	5.47	5.32	5.53	3.76	6.43	5.75	8.02	5.46	6.11	4.35	4.93	3.54	4.01	0.12	3.61	1.43	0.33	4.68	4.11	3.66
Il	0.30	0.26	0.25	0.21	0.30	0.30	0.32	0.29	0.28	0.39	0.21	0.24	0.18	0.18	0.20	0.14	0.13	0.20	0.20	0.18
Hm	12.22	9.74	8.61	8.56	8.80	8.99	8.15	9.55	7.00	8.59	6.97	7.27	6.14	5.50	6.92	5.80	5.97	6.77	6.78	6.67
Ap	2.56	1.31	1.66	2.02	0.78	0.87	1.59	0.59	1.71	0.84	1.76	1.47	1.87	2.74	1.58	2.69	2.44	1.69	1.68	1.56
Bi	17.22	19.22	15.86	13.36	22.33	15.75	14.85	22.59	16.16	19.25	9.77	13.26	8.71	8.56	11.05	8.35	8.93	10.18	10.09	11.77
Hbl																				
Sum	98.45	98.57	98.42	98.22	99.08	98.02	99.01	99.31	98.49	98.80	98.17	98.24	97.86	97.29	98.14	97.42	97.34	98.19	98.12	98.04

Continue...

Table 2. Continuation.

%	SOS 860B	SOS 860C	SOS 853M	SOS 861R	SOS 861E	SOS 853N	SOS 861J	SOS 861N	SOS 861I	SOS 861F	SOS 861T	SOS 861G	SOS 853J	SOS 853E	SOS 861D	SOS 848B	SOS 860F	SOS 861C	SOS 853F
SiO ₂	58.79	58.89	58.93	59.16	59.33	59.58	59.64	59.80	60.39	60.62	60.62	60.65	60.89	60.91	60.97	61.70	61.72	61.98	61.98
TiO ₂	1.08	0.63	0.56	0.68	0.75	0.69	0.68	0.74	0.65	0.65	0.68	0.68	0.70	0.78	0.62	0.83	0.58	0.58	0.52
Al ₂ O ₃	15.26	14.73	14.49	15.14	15.00	15.32	15.18	15.39	14.99	14.92	14.91	15.08	14.85	15.14	15.03	15.38	14.97	14.87	14.94
Fe ₂ O ₃	6.92	7.11	7.81	5.90	6.73	6.94	6.53	6.36	6.11	6.30	6.03	6.31	6.27	5.80	6.31	6.16	5.67	5.87	6.11
MnO	0.11	0.10	0.13	0.08	0.09	0.08	0.09	0.09	0.08	0.09	0.07	0.08	0.09	0.08	0.08	0.08	0.07	0.09	0.09
MgO	3.88	4.05	5.09	2.80	3.60	3.61	3.05	3.15	2.86	3.30	2.74	3.19	3.46	2.68	3.37	3.08	2.80	3.07	3.22
CaO	4.91	4.84	5.37	4.53	4.35	4.94	4.10	3.91	4.10	4.16	4.08	3.73	4.30	3.59	4.23	4.69	3.70	3.69	4.52
Na ₂ O	4.06	3.61	4.39	3.43	3.65	4.30	3.90	3.80	3.81	3.72	4.10	3.65	4.20	4.11	4.06	4.19	3.86	3.75	4.55
K ₂ O	3.38	4.30	2.05	6.09	4.54	2.72	4.73	4.56	4.94	4.36	4.65	4.54	3.34	4.48	3.45	3.48	4.57	4.26	2.33
P ₂ O ₅	0.71	0.62	0.33	0.66	0.66	0.50	0.71	0.71	0.65	0.53	0.70	0.69	0.58	0.89	0.52	0.56	0.55	0.44	0.40
LOI	0.82	0.50	0.65	0.92	0.73	0.49	0.67	0.70	0.69	0.75	0.76	0.77	0.58	0.74	0.83	0.45	0.61	0.57	0.75
Total	99.90	99.38	99.80	99.38	99.43	99.18	99.28	99.21	99.26	99.40	99.33	99.38	99.25	99.19	99.47	100.59	99.12	99.17	99.41
Q	15.12	14.68	17.30	10.29	14.60	16.44	13.29	14.59	13.86	16.17	13.76	16.59	17.36	15.18	17.65	17.01	16.42	18.11	19.43
Or	11.03	16.11	0.42	29.55	18.55	7.73	20.95	19.71	22.59	18.18	21.18	19.47	11.78	20.28	12.62	13.47	20.59	18.09	6.38
Ab	34.31	30.56	37.12	28.99	30.88	36.40	33.02	32.14	32.27	31.48	34.67	30.87	35.50	34.80	34.33	35.44	32.66	31.77	38.47
An	13.47	11.27	13.76	7.93	11.12	14.48	9.94	11.46	9.21	11.12	8.54	11.36	11.83	9.63	12.59	12.89	10.01	11.15	13.48
Wo	2.61	3.62	4.47	4.26	2.56	2.84	2.42	1.37	2.87	2.53	2.99	1.09	2.38	1.00	2.08	2.80	1.98	1.78	2.63
Il	0.23	0.21	0.27	0.17	0.19	0.18	0.19	0.19	0.18	0.19	0.16	0.17	0.18	0.16	0.18	0.16	0.16	0.20	0.19
Hm	6.92	7.11	7.81	5.90	6.73	6.94	6.53	6.36	6.11	6.30	6.03	6.31	6.26	5.80	6.31	6.16	5.67	5.87	6.11
Ap	1.68	1.47	0.79	1.57	1.56	1.17	1.67	1.68	1.53	1.25	1.65	1.64	1.36	2.10	1.23	1.32	1.30	1.04	0.95
Bi	12.80	13.36	16.80	9.24	11.89	11.93	10.06	10.40	9.44	10.91	9.03	10.53	11.43	8.84	11.14	10.17	9.23	10.13	10.62
Sum	98.16	98.39	98.76	97.91	98.09	98.13	98.08	97.9	98.06	98.14	98.02	98.06	98.09	97.80	98.14	99.43	98.04	98.15	98.26

LOI: loss on ignition.

$$C_i^h - C_f^i = m(C_m^i - C_f^i) \quad (1)$$

C_m^i = the concentration in the mafic magma;
 m = the fraction of the mafic magma in the mixture.

Where:

C_i^h = the concentration of element i in the hybrid magma;

C_f^i = the concentration in the felsic magma;

Using the algorithm by Fourcade and Allegre (1981), the samples SOS 850B (48% SiO₂) and SOS 854 (72.6% SiO₂,

Table 3. Representative chemical analysis of trace elements of RJB MEs. Values are in parts per million.

	SOS 850B	SOS 876B	SOS 867B	SOS 849B	SOS 844B	SOS 861M	SOS 853D	SOS 861P	SOS 861E	SOS 861T	SOS 848B	SOS 861C
Ba	1,162	626	770	564	300	819	655	819	947	896	817	862
Rb	208.4	98.8	158.0	120.0	174.0	234.0	132.5	233.0	233.0	243.0	115.5	213.0
Sr	969	683	540	678	316	463	585	450	491	489	561	521
Zr	271	230	237	228	177	240	196	242	250	242	264	212
Nb	15.35	10.70	9.80	8.74	13.00	11.00	12.36	11.40	10.50	11.30	9.60	11.00
La	50.4	34.5	45.1	33.2	18.8	45.9	35.4	48.2	41.5	42.0	43.5	46.9
Ce	109.3	76.9	80.4	72.3	46.3	98.2	78.4	104.0	95.4	90.9	88.8	84.1
Pr	14.41	9.48	8.28	9.35	5.97	11.45	10.28	12.05	11.35	10.7	10.25	10.2
Nd	64.8	38.6	29.3	41.7	22.9	42.5	44.2	45.6	44.9	40.2	37.0	37.9
Sm	13.1	7.39	5.82	8.80	4.80	7.66	8.40	8.29	8.25	6.90	7.24	6.93
Eu	3.34	2.16	1.32	1.70	1.35	1.29	2.02	1.36	1.39	1.28	1.32	1.69
Gd	10.37	6.74	4.10	6.70	3.79	5.30	6.49	5.60	5.37	4.80	4.67	5.27
Tb	1.23	0.83	0.46	0.83	0.41	0.53	0.84	0.65	0.62	0.50	0.52	0.57
Dy	5.85	4.37	2.62	4.15	2.57	3.14	4.05	2.89	3.17	3.02	2.93	3.3
Ho	0.82	0.85	0.46	0.69	0.47	0.51	0.71	0.51	0.55	0.45	0.53	0.57
Er	2.12	2.16	1.32	2.01	1.35	1.29	1.95	1.36	1.39	1.28	1.32	1.69
Tm	0.24	0.27	0.18	0.28	0.21	0.18	0.27	0.19	0.20	0.16	0.21	0.22
Yb	1.50	1.70	0.99	1.70	1.38	0.92	1.70	1.01	1.11	1.13	1.03	1.32
Lu	0.20	0.29	0.19	0.23	0.23	0.19	0.26	0.18	0.17	0.17	0.19	0.20
Y	24.23	20.30	11.20	19.84	13.20	13.30	21.30	13.40	13.40	12.70	13.00	14.80
Cs	25.00	5.82	7.30	10.36	13.15	13.40	6.71	15.15	17.00	18.65	4.74	14.15
Ta	0.71	0.90	0.70	0.44	0.90	0.90	0.92	0.80	0.70	1.00	0.80	0.90
Hf	7.96	5.80	6.10	6.55	5.50	6.00	5.88	6.40	6.20	6.00	6.70	5.60
Ga	31.9	23.7	23.6	27.1	29.7	24.8	27.1	25	24	25.3	24.2	25.1
Sn	8.4	4.0	6.0	4.1	9.0	5.0	1.1	5.0	4.0	4.0	4.0	4.0
Th	8.40	5.66	9.86	4.60	5.81	10.80	8.80	11.25	9.59	9.84	13.10	10.80
V	227	172	137	133	118	113	110	120	123	102	125	98
W	4.9	276.0	274.0	< 0.1	4.0	720.0	< 0.1	693.0	529.0	542.0	7.0	428.0
Eu/Eu*	0.88	0.82	0.48	0.68	0.65	0.81	0.84	0.81	0.81	0.87	0.77	0.76
(La/Yb) _N	22.40	9.61	30.37	13.02	9.08	33.26	13.88	31.82	24.92	24.78	28.16	23.69
(La/Sm) _N	2.37	2.04	4.77	2.32	2.41	3.69	2.59	3.58	3.09	3.74	3.70	4.16

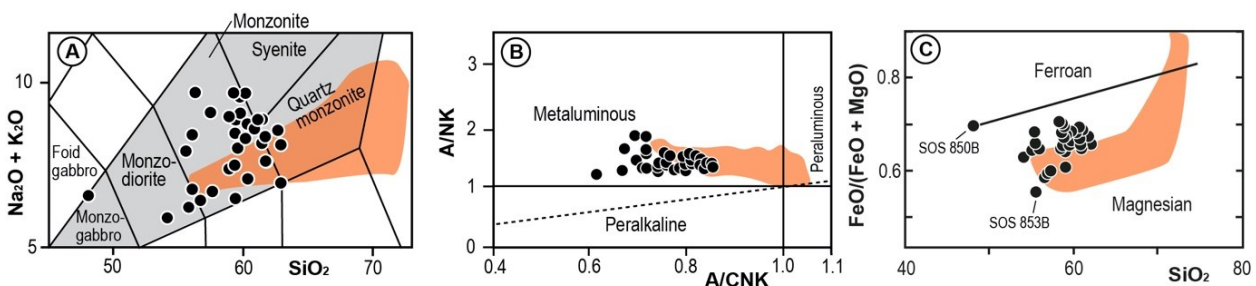


Figure 7. Chemical classification diagram applied to the RJB MEs. (A) Na₂O + K₂O versus SiO₂ diagram with fields defined by Middlemost (1985). (B) Aluminum saturation A/CNK (Al₂O₃/(CaO + Na₂O + K₂O)) versus A/NK (Al₂O₃/(Na₂O + K₂O)) diagram of Maniar and Picolli (1989). (C) FeO/(FeO+MgO) versus SiO₂ diagram (Frost *et al.* 2001). The orange area corresponds to the RJB rocks, and the gray area, in diagram A, represents the field of medium alkalinity rocks.

obtained from Sousa *et al.* 2019) were considered as representatives of the mafic and felsic magmas, respectively. To represent the hybrid magma, ME SOS 816C, which has a relatively high SiO₂ content (61.9%), was used, because it is the ME with the highest degree of hybridization (high SiO₂ and low V). A good linear correlation was obtained with the analyzed rocks, with R² = 0.991 (Fig. 10B). The angular coefficient obtained represents the fraction of the mafic magma involved in the mixing; for the SOS 816C sample, it is 43%.

Mingling

According to Perugini and Poli (2012), the evolution of the rheological contrast between magmas can be rebuilt from the study of magmatic enclaves. The various forms of MEs can be controlled by the differences in the viscosities/rheologies of the magmas, and the more complex the forms, the greater these differences will be (Fernandez and Barbarin 1991, Perugini and Poli 2011). According to Petford (2003), several studies estimate that, regardless of composition, the transition from Newtonian to non-Newtonian behavior for magmas occurs when the magma is between 30% and 50% crystallized. Fernandez and Barbarin (1991) acknowledged that the injection of mafic magma at different stages of felsic magma crystallization can generate varied structures:

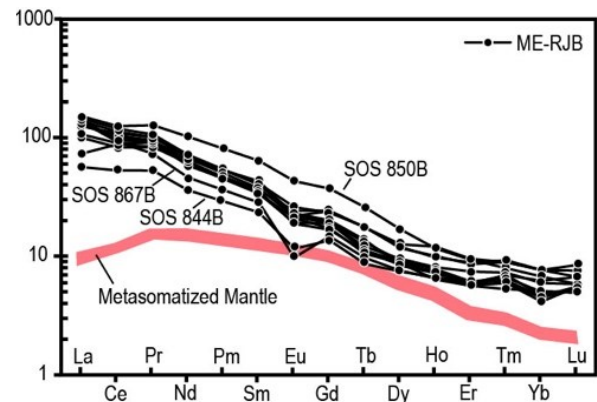
- when the felsic host magma has a Newtonian behavior (up to 30% crystallized), active convection induces the dispersion of mafic magma droplets, generating globular MEs;
- when the felsic magma has a viscoplastic behavior (30 to ~50% crystallized), the ME shapes can be deformed;
- when the felsic magma is 70–90% crystallized, early fractures can be formed and allow the mafic magma to be injected, which will result in syn-plutonic dikes.

The formation of these syn-plutonic dikes can occur in two ways, depending on their thickness. When the mafic magma is injected as thin dikes, it quickly reaches a thermal balance by cooling down and becoming rigid. During the subsequent movements of the host magma, the dikes are broken, resulting in a syn-plutonic dike composed of MEs with angular contacts. When the mafic dike is thicker, its cooling is slower and it can overheat the host magma at the contacts, which will undergo limited partial melting. Local convection, caused by the increase in the thermal gradient, will induce the dispersion

of the mafic magma as bubbles of various sizes, transforming the mafic dike into a corridor of MEs (syn-plutonic dike).

In the RJB, MEs with globular, elongated shapes and well-defined contacts (crenulated, cusped, lobate, and sinuous) are found, in addition to syn-plutonic dikes composed of various enclaves of different shapes and sizes. These features indicate that mafic magmas were injected during two different crystallization stages in the RJB magmatic chamber. According to the model of Fernandez and Barbarin (1991), MEs with globular shapes were formed when mafic magma was injected into the felsic magmatic chamber of the RJB, with up to 30% crystallized, and disaggregated by convective movements; this also agrees with the interpretations of other authors about the genesis of globular MEs (e.g., Vernon *et al.* 1988, Castro *et al.* 1991, Liu *et al.* 2013, Shukla and Mohan 2019). Since MEs with such features are well distributed throughout the RJB, we believe that the input of mafic magma in this stage was important. It is believed that the RJB MEs with crenulated, cusped, lobate, and sinuous contacts were formed when the felsic magmatic chamber had a degree of crystallization greater than 30%, as a greater difference in viscosity is necessary to generate these more complex forms (e.g., Perugini and Poli 2011). The input of mafic magma was probably more restricted at this stage, as enclaves with these types of contacts in the RJB only occur in the western region of the batholith.

The syn-plutonic dikes observed in the RJB indicate the occurrence of mafic magma pulses in the late stages of



ME-RJB: microgranular enclaves of the Rio Jacaré Batholith.

Figure 9. Chondrite-normalized (Nakamura 1974) REE diagram for the RJB MEs. Composition of the metasomatized mantle of Kaczmarek *et al.* (2016).

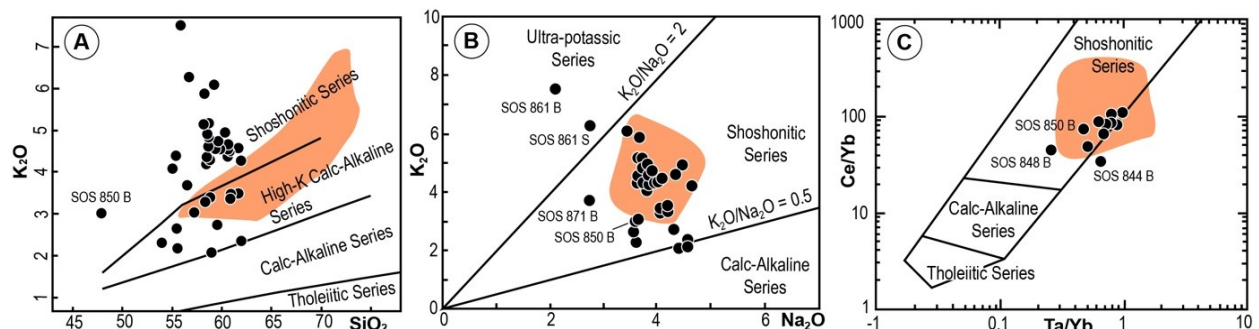


Figure 8. Geochemical diagrams for magmatic affinity inference. (A) K₂O versus SiO₂ diagram of Peccerillo and Taylor (1976). (B) K₂O versus Na₂O diagram of Turner *et al.* (1996), characterizing the nature of the ME magma. (C) Ta/Yb versus Ce/Yb, with fields defined by Pearce (1982). The orange area corresponds to the RJB compositions.

crystallization, when 70–90% of the felsic magmatic chamber was crystallized, and that the presence of this mafic magma increased the local temperature, provoking the partial melting of the felsic magma. It is suggested that the contribution of mafic magma in the late stages of the crystallization of the RJB was restricted, as the syn-plutonic dikes are limited to the western region. The RJB's multiple ME types also suggest the occurrence of more than one mafic magmatic pulse during the evolution and formation of this batholith.

Some textures found in the RJB MEs also indicate that these enclaves probably represent the breakdown of the mafic magma that was injected and cooled in a cooler felsic magmatic chamber:

- zones of inclusion in plagioclase and ocellar quartz crystals (Hibbard 1991);
- a boxy cellular plagioclase texture (Hibbard 1991);
- acicular apatite (Wyllie *et al.* 1962, Hibbard 1991).

According to Torkian and Furman (2015), these textures and the crenulated and cusped contacts between the MEs and the host rocks can be attributed to the mingling/mixing of magmas.

Feldspar and quartz xenocrystals in the ME can be observed in the field. The presence of xenocrystals in these enclaves indicates that the phenocrysts of the host magma surpassed the ME edges and were trapped inside (Barbarin and Didier 1991, Perugini *et al.* 2003). This indicates that the mafic and felsic magmas interacted with each other and had different rheologies, allowing the exchange of crystals between them in a mingling process (e.g., Perugini *et al.* 2003, Yang *et al.* 2015).

Therefore, it is suggested that the studied rocks are a product of partial chemical equilibrium between mafic and felsic magmas, representing a mingling/mixing process.

Magma of the microgranular enclaves

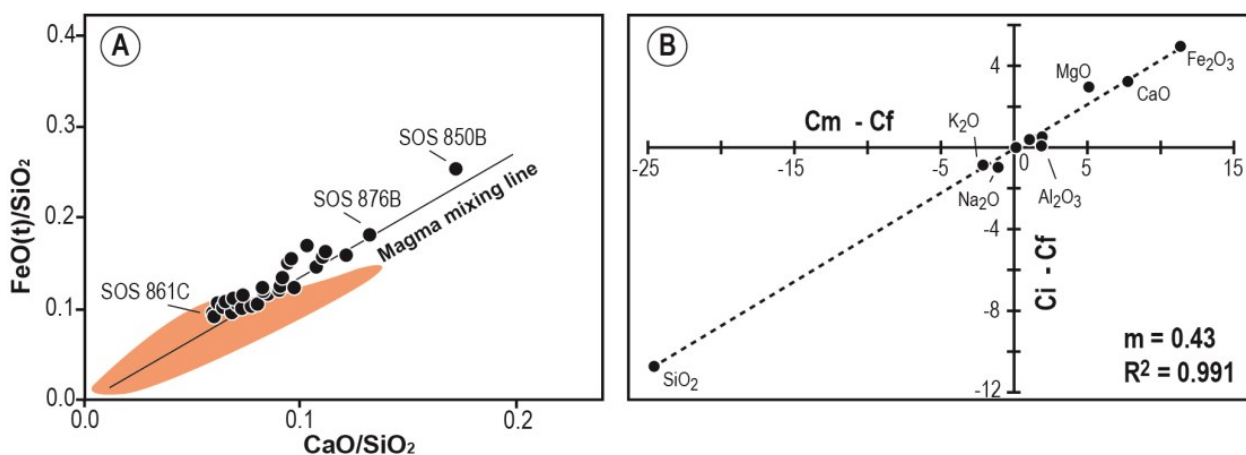
MEs in granites have been interpreted (e.g., Bonin 2004, Janoušek *et al.* 2004, Chen *et al.* 2007) as mantle-derived mafic magmas that underwent mixing/mingling after being injected

into a deep crustal felsic magmatic chamber. The chemical compositions of the MEs studied reveal their affinity with the magnesian series and indicate that this mafic magma was hydrated and crystallized in an oxidizing environment, as suggested by Frost and Lindsay (1991) for rocks in this series. High fO_2 can also be inferred from the presence of titanite, quartz, magnetite, and hornblende (e.g., Wones 1989). Furthermore, most of the RJB MEs have high K_2O , with $K_2O/Na_2O > 1$, which is the characteristic of shoshonitic rocks (Figs. 8A–8C). K_2O is high regardless of the rocks' SiO_2 content, and according to Turner *et al.* (1996), rocks with these characteristics probably reflect a potassium phase not only during fractionation but also at the source.

According to Furman and Graham (1999), an increase in the Rb/Sr ratio in relation to the primitive mantle may suggest that phlogopite was the hydrated mineral present at the source, while high Ba/Rb ratios suggest the presence of amphibole. The Rb/Sr ratios of the RJB MEs range from 0.14 to 0.55, and the primitive mantle has a ratio of 0.03 (Sun and McDonough 1989), suggesting mingling and can also indicate that the phlogopite in the source participated in the partial melt responsible for the magmas that generated the studied MEs (Fig. 11).

Shoshonitic magmas have as their main source the subcontinental lithospheric mantle or the asthenospheric mantle, which were both previously enriched in incompatible elements by subduction (e.g., Aldanmaz *et al.* 2000). The studied MEs show depletion in Ti, Nb, and Ta (Fig. 12) and high Th/Yb ratios, which are typical signatures of magmas generated in an orogenic environment and represent contributions from the subducted plate (e.g., Foley and Wheller 1990, Ringwood 1990, Pearce 2008). RJB MEs have higher Th/Yb ratios than mantle evolution curves defined for MORBs and OIBs, which suggest subduction-induced source metasomatism (Fig. 13). The Hf, Th, Zr, Ce, and Nb content of the studied rocks indicates that this magma is formed in a post-collisional orogenic environment (Figs. 14A and 14B).

High LILE and high Ba/Nb (> 13) and Ba/La (> 8) ratios are suggestive of enriched mantle sources (Ryan *et al.* 1996, Kepezhinskas *et al.* 2016). Such ratios in the RJB MEs are above

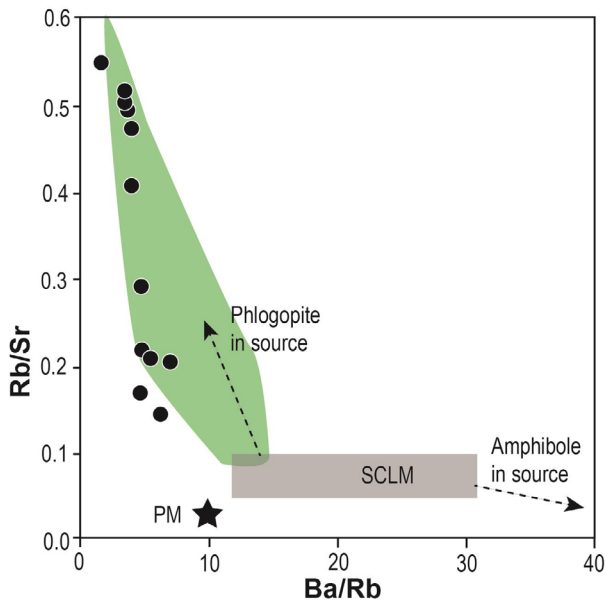


Cf: element concentration in felsic magma; Cm: element concentration in mafic magma; Ci: element concentration in hybrid magma; m: fraction of mafic magma in the mixture; R²: correlation coefficient.

Figure 10. Geochemical diagrams used to simulate the mixture of mafic and felsic magmas. (A) CaO/SiO₂ versus FeO/SiO₂ diagram of Berzina *et al.* (2014). (B) Test diagram of the mixing of larger elements of Fourcade and Allegre (1981), which indicate the role of the mixing of the ME and RJB magmas. The orange area corresponds to the RJB compositions.

23 and 15, respectively, so they are compatible with enriched mantle sources. In addition, the low values of the Nb/La ratios (0.22–0.69) are consistent with a lithospheric mantle source (Fig. 15).

Sample SOS 850B is considered to be the most primitive of the RJB MEs, without evidence of cumulative texture, low SiO₂ content (48%), moderate MgO (5.2%), and high CaO (8.2%) and V (227 ppm). It is also the only sample that presents normative olivine. Although the MgO content of this sample is not the highest among the MEs, its composition is similar to the compositions described for shoshonitic basalts (Morrison 1980) or trachybasalts of the Roman Province (Müller and Groves 2019). When calculating the partial melting of the metasomatized mantle by using the mantle composition (which consists of clinopyroxene (43%), amphibole (34%), phlogopite (22%), and spinel (1%)) of Kaczmarek *et al.* (2016), employing the batch melting model, the result points to a partial melting rate of less than 3% to generate magmas with compositions similar to that of sample SOS 850B (Table 4 and Fig. 16). According to Conceição and Green (2004), low melting rates are necessary



SCLM: subcontinental lithospheric mantle; PM: primitive mantle (Sun and McDonough 1989).

Figure 11. Ba/Rb versus Rb/Sr diagram after Furman and Graham (1999), suggesting the presence of phlogopite in the mantle source of the RJB MEs. The green area represents the compositions of the other SOS MEs.

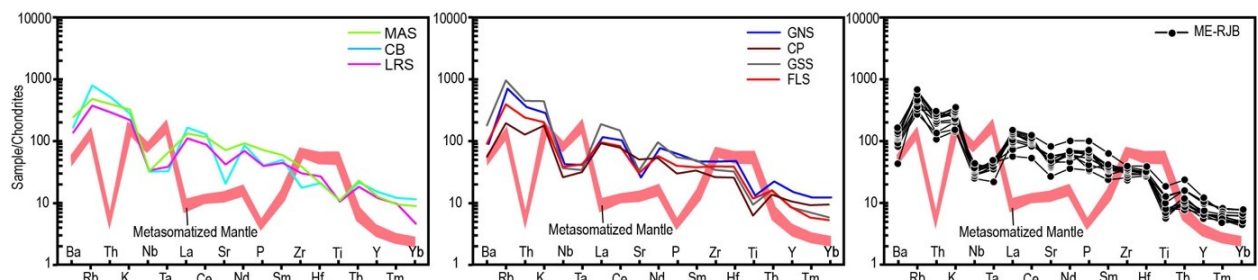


Figure 12. Chondrite multi-elemental diagrams for the RJB MEs (Thompson 1982). Composition of the metasomatized mantle from Kaczmarek *et al.* (2016). The colored lines correspond to the average compositions from enclaves of the Glória Norte Stock [GNS; Lisboa *et al.* 2019]; Curitiba Batholith [CB; Gentil 2013]; Lagoa do Roçado Stock [LRS; Silva 2014]; Monte Alegre Stock [MAS; Oliveira 2014]; Glória Sul Stock [GSS; Conceição *et al.* 2016]; Capela Pluton [CP; Pereira *et al.* 2019]; and Fazenda Lagoas Stock [FLS; Fernandes *et al.* 2020].

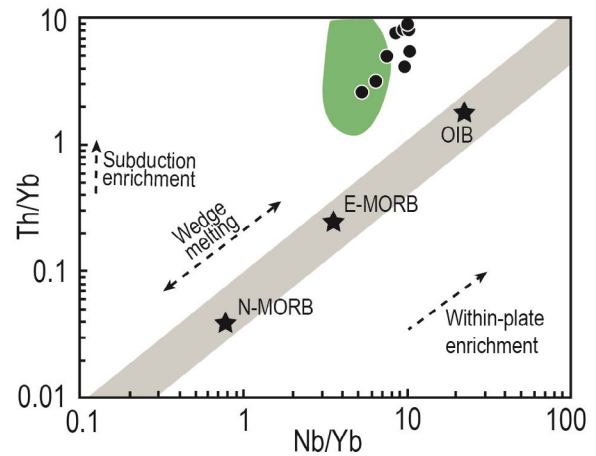


Figure 13. Nb/Yb versus Th/Yb diagram (Pearce 2008) applied to the RJB MEs. The green area represents the compositions of other SOS MEs.

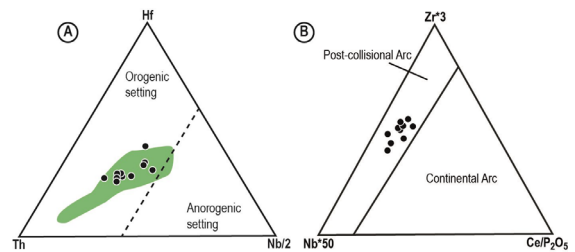


Figure 14. (A) Hf-Th-Nb/2 diagram (Křmíček *et al.* 2011) and (B) Nb*50 – Zr*3 – Ce/P₂O₅ diagram (Müller *et al.* 1992) applied to the RJB MEs, showing the post-collisional orogenic affinity. The green area represents the compositions of other SOS MEs.

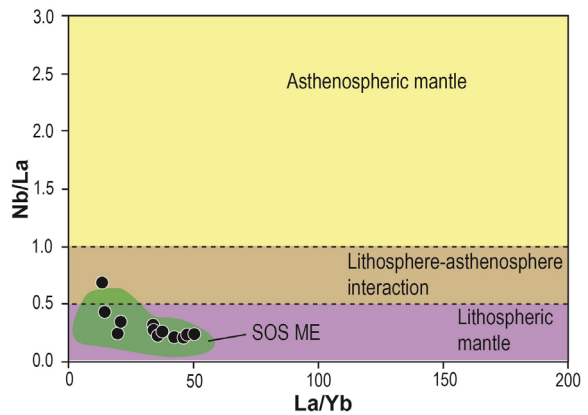


Figure 15. La/Yb versus Nb/La diagram (Smith *et al.* 1999) applied to the RJB MEs.

for the formation of shoshonitic magmas; this is consistent with the values obtained in this work.

Sousa *et al.* (2019) found normal zoning in plagioclase crystals of the RJB MEs. This type of zoning in plagioclase suggests that magmatic fractionation occurs during the process of mixing magmas. The occurrence of pronounced valleys in Ba and Sr, and the negative Eu anomalies in multielementary diagrams (Fig. 12) may indicate the fractionation of plagioclase. The predominance of P peaks (Fig. 12) may suggest the chemical diffusion of P from the host magma to the enclave magma, leading to the crystallization of apatite (Nardi and Lima 2000). The decrease in the P_2O_5 and (La + Ce) content with the evolution of the ME magma supports the assumption that the fractional crystallization of apatite was an active process (Fig. 17).

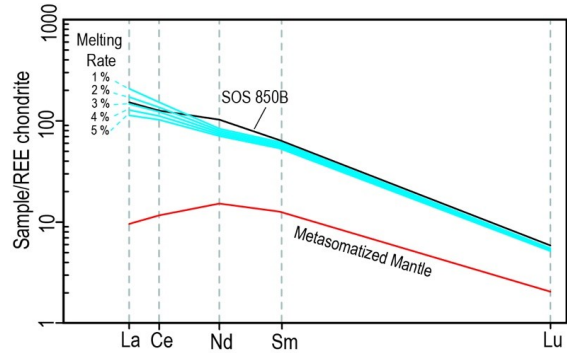


Figure 16. Chondrite multi-elemental diagram (Nakamura 1974) of the partial melting of the metasomatized mantle (Kaczmarek *et al.* 2016). The blue lines were obtained from the batch melting calculation. The partition coefficients used in the calculation are from Foley *et al.* (1996), Zack *et al.* (1997), Grégoire *et al.* (2000), and Elkins *et al.* (2008).

Table 4. Values obtained from the calculation of the partial melting of the metasomatized mantle (MM; Kaczmarek *et al.* 2016) using the batch melting method. Partition coefficients in the calculations from Foley *et al.* (1996), Zack *et al.* (1997), Grégoire *et al.* (2000), and Elkins *et al.* (2008).

	PM 1 %	PM 2 %	PM 3%	PM 4 %	PM 5 %	MM	SOS 850B
La	68.75	56.87	48.49	42.26	37.45	3.17	50.4
Ce	132.17	117.79	106.23	96.74	88.80	10.10	109.3
Nd	52.77	50.49	48.39	46.46	44.68	9.62	64.8
Sm	12.56	12.09	11.65	11.24	10.86	2.58	13.1
Lu	0.19	0.18	0.18	0.17	0.17	0.07	0.2

PM: partial melting rate.

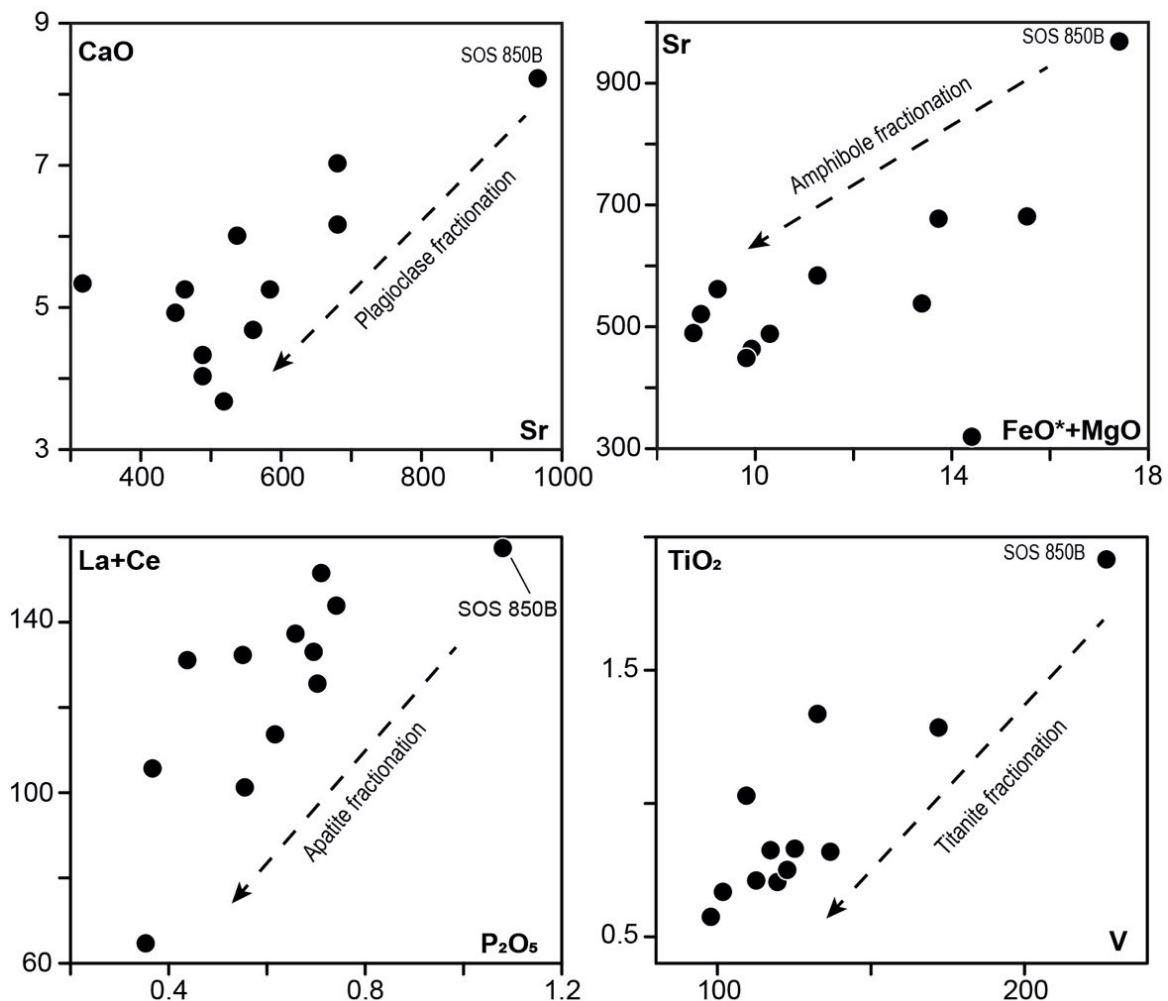


Figure 17. Binary Sr versus CaO, (FeO* + MgO) versus Sr, P_2O_5 versus (La + Ce), and V versus TiO_2 diagrams applied to the RJB MEs, showing vectors that correspond to the fractionation of plagioclase, amphibole, apatite, and titanite.

The Ti valleys in multielementary diagrams, in addition to representing a signature of the magmatic source, also suggest the fractionation of titanite and opaque minerals. By observing the behavior of compatible elements in some minerals (Sr and CaO in plagioclase, Sr and (FeO* + MgO) in amphibole, P₂O₅ and (La + Ce) in apatite and V and TiO₂ in titanite) and the degree of ME magma evolution, it was observed that there is a decrease in these chemical elements with the evolution of the ME magmas (Fig. 17). This reinforces the hypothesis that the fractional crystallization of these minerals may have also contributed to the compositional variation of the MEs studied.

Inference about the nature of mafic magmas in the Sergipano Orogenic System

In the SOS, MEs are found mainly in intrusions of the Macururé and Poço Redondo domains, such as in the Glória Norte Stock (Lisboa *et al.* 2019), Curitiba Batholith (Gentil 2013, Lima 2016), Lagoa do Roçado Stock (Silva 2014), Monte Alegre Stock (Oliveira 2014), Glória Sul Stock (Conceição *et al.* 2016), Fazenda Lagoas Stock (Fernandes *et al.* 2020), RJB (Sousa *et al.* 2019), and Capela Stock (Pereira *et al.* 2019). Many of these plutons are more than 10 km apart and have ages varying from 631 to 588 Ma.

The geochemical data of the studied samples were compared with those ME of other plutons of the SOS. The geochemistry indicated that all these MEs are metaluminous and magnesian, and they have shoshonitic affinity. The abundances of trace elements and REEs in the MEs are also similar, and this is reflected by similar incompatible element patterns (Fig. 12).

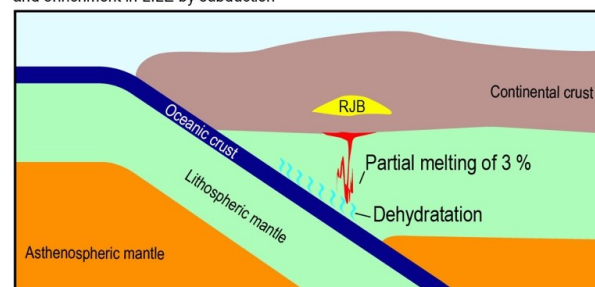
Despite their different ages, the MEs from the Macururé and Poço Redondo plutons have similar characteristics, which suggest that the mafic magma responsible for the formation of these MEs had a similar source to the magma of the RJB MEs: the lithospheric mantle enriched in incompatible elements. This type of source was also attributed to K-diorites from the Borborema Province by Hollanda *et al.* (2003) and is confirmed when comparing the variation of the (⁸⁷Sr/⁸⁶Sr)_i ratios (between 0.7059 and 0.71202) and of ε_{Nd} (from -9.3 to -20.1). It is likely that the source of the RJB MEs is the same as the source described by Hollanda *et al.* (2003) for the potassic mafic magmas of the Borborema Province.

CONCLUSIONS

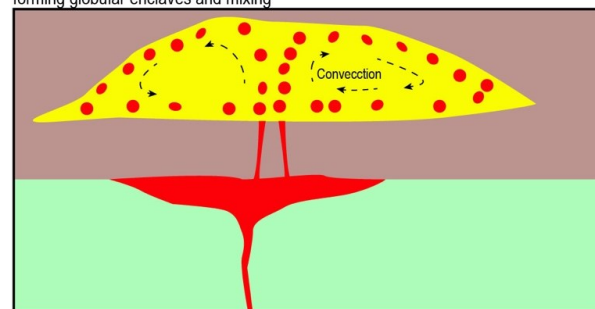
The origin of the RJB MEs can be summarized in four steps (Fig. 18):

- Step 1: A 3% rate of partial melting of the lithospheric mantle previously enriched in incompatible elements by subduction, originating the shoshonitic mafic magma responsible for the generation of the MEs of the RJB;
- Step 2: The injection of this mafic magma when the RJB magmatic chamber had crystallization rates ranging from 0 to 30% allowed mixing between these magmas, the disaggregation of the mafic magma by convection currents, and the subsequent formation of MEs with globular shapes throughout the RJB;
- Step 3: New injections of shoshonitic mafic magma, which occurred when the RJB magmatic chamber was more than

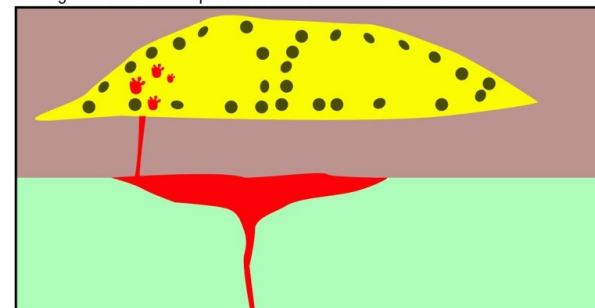
Stage I - Origin of the mafic magma by partial melting of 3 % of the lithospheric mantle and enrichment in LILE by subduction



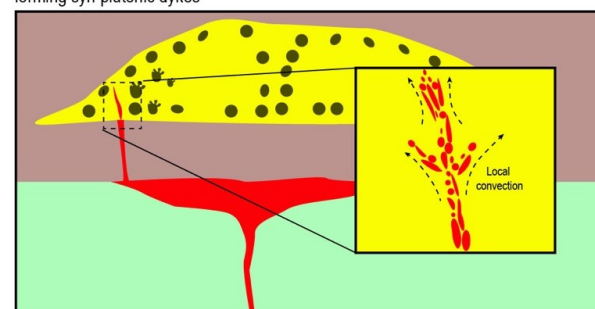
Stage II - Injection of the magma mafic in RJB magma chamber < 30 % crystallized forming globular enclaves and mixing



Stage III - Injection of the magma mafic in RJB magma chamber > 30 % crystallized forming enclaves with complex forms and crenulated contacts



Stage IV - Injection of the magma mafic in RJB magma chamber 70-90 % crystallized forming syn-plutonic dykes



Mafic magma: red color; MEs: black color.

Figure 18. Schematic model of the different steps of the formation of MEs in the RJB.

- 30% crystallized, generating MEs with complex shapes and crenulated, sinuous and cusped contacts in the western region of the batholith;
- Step 4: The late injection of mafic magma in the western region of the RJB magmatic chamber (which was 70–90% crystallized) resulted in the formation of syn-plutonic dikes.

The chemical data of the studied MEs suggest that the mixing between the ME mafic magma and the RJB felsic magma was important, and also that the smallest fraction of mafic magma involved in this process was 43%. Mixing was responsible for the generation of MEs with various colors (black to

gray) and contributed to the compositional variation of these rocks, which have diorite, monzodiorite, quartz monzodiorite, and monzonite compositions. Furthermore, the fractionation of plagioclase, hornblende, titanite, and apatite may have also contributed to the compositional variation of the RJB MEs.

ACKNOWLEDGMENTS

This study was carried out with the support from the Coordenação de Aperfeiçoamento de Pessoal de Nível Superior — Brazil (CAPES) — Financing Code 001. Carlos

Santana Sousa and Hiakan Santos Soares thank CNPq for their PhD scholarships, whose processes are 163770/2018-2 and 169765/2018-0, respectively. Herbet Conceição and Maria de Lourdes Rosa are fellows of the Brazilian National Council for Scientific and Technological Development (CNPq). The authors are grateful for the support of the Laboratory of Petrology Applied to Mineral Research at the Universidade Federal de Sergipe in the development of the research. They are also grateful to the anonymous reviewers for comments and suggestions that have considerably improved the original manuscript.

ARTICLE INFORMATION

Manuscript ID: 20220033. Received on: 13 APR 2022. Approved on: 29 JULY 2022.

How to cite: Sousa C.S., Soares H.S., Rosa M.L.S., Conceição H. 2022. Injections of enriched lithospheric mantle magmas explain the formation of microgranular enclaves in the Rio Jacaré Batholith, Borborema Province, Brazil. *Brazilian Journal of Geology*, 52(4):e20220033. <https://doi.org/10.1590/2317-4889202220220033>

C.S. wrote the manuscript, compiled data from microgranular enclaves of the Sergipe Orogenic System, and prepared the tables and figures for the article. H.C. and M.R. helped in the development of fieldwork and analytical costs were largely financed by projects under their coordination; they contributed to discussions and suggestions during the course of the research. H.S. helped in fieldwork, in the treatment and processing of samples, in the elaboration of some diagrams, and in constructive discussions on the topic addressed.

Competing interest: the authors declare no competing interests.

REFERENCES

- Aldanmaz E., Pearce J.A., Thirlwall M.F., Mitchell J.G. 2000. Petrogenetic evolution of late Cenozoic, post-collisional volcanism in western Anatolia, Turkey. *Journal of Volcanology and Geothermal Research*, 102(1-2):67-95. [https://doi.org/10.1016/S0377-0273\(00\)00182-7](https://doi.org/10.1016/S0377-0273(00)00182-7)
- Almeida F.F.M., Hasuí Y., Brito Neves B.B., Fuck R.A. 1977. Províncias estruturais brasileiras. In: Simpósio de Geologia do Nordeste, Campina Grande. *Anais...*, p. 363-391.
- Barbarin B., Didier J. 1991. Macroscopic features of mafic microgranular enclaves. In: Didier J., Barbarin B. (eds.). *Enclaves in Granite Petrology (Development in Petrology)*. Amsterdam: Elsevier, p. 253-262.
- Berzina A.P., Berzina A.N., Gimon V.O. 2014. Geochemical and Sr–Pb–Nd isotopic characteristics of the Shakhtama porphyry Mo–Cu system (Eastern Transbaikalia, Russia). *Journal of Asian Earth Sciences*, 79(Part B):655-665. <https://doi.org/10.1016/j.jseae.2013.07.028>
- Bonin B. 2004. Do coeval mafic and felsic magmas in post-collisional to within-plate regimes necessarily imply two contrasting, mantle and crustal, sources? A review. *Lithos*, 78(1-2):1-24. <https://doi.org/10.1016/j.lithos.2004.04.042>
- Brito M.F. (1996). *Geologia, geoquímica e petrologia do Complexo Granítico Sítios Novos, Sistema de Dobramentos Sergipano*. MS Dissertation, Universidade Federal de Pernambuco, Recife.
- Bueno J.F., Oliveira E.P., McNaughton N.J., Laux J.H. 2009. U-Pb dating of granites in the Neoproterozoic Sergipano Belt, NE-Brazil: Implications for the timing and duration of continental collision and extrusion tectonics in the Borborema Province. *Gondwana Research*, 15(1):86-97. <https://doi.org/10.1016/j.gr.2008.06.003>
- Carvalho M.J. (2005). *Evolução tectônica do Domínio Maracó-Poço Redondo: Registro das Orogêneses Cariris Velhos e Brasileira na Faixa Sergipana, NE do Brasil*. PhD Thesis, Universidade de Campinas, Campinas, 202 p.
- Castro A., Moreno-Ventas I., De La Rosa J.D. 1991. H-type (hybrid) granitoids: a proposed revision of the granite-type classification and nomenclature. *Earth-Science Reviews*, 31(3-4):237-253. [https://doi.org/10.1016/0012-8252\(91\)90020-G](https://doi.org/10.1016/0012-8252(91)90020-G)
- Chen B., Zhai M.G., Tian W. 2007. Origin of the Mesozoic Magmatism in the North China Craton: constraints from petrological and geochemical data. *Geological Society*, 280(1):131-151. <https://doi.org/10.1144/SP280.6>
- Chen Y.D., Price R.C., White A.J.R., Chappell B.W. 1990. Mafic inclusions from the Glenbog and Blue Gum Granite Suites, southeastern Australia. *Journal of Geophysical Research*, 97(B11):17757-17785. <https://doi.org/10.1029/jb095ib11p17757>
- Clemens J.D., Elburg M.A., Harris C. 2017. Origins of igneous microgranular enclaves in granites: the example of Central Victoria, Australia. *Contributions to Mineralogy and Petrology*, 172:88. <https://doi.org/10.1007/s00410-017-1409-2>
- Conceição J.A., Rosa M.L.S., Conceição H. 2016. Sienogranitos leucocráticos do Domínio Macururé, sistema Orogênicos Sergipano, nordeste do Brasil: stock Glória Sul. *Brazilian Journal of Geology*, 46(1):63-77. <https://doi.org/10.1590/2317-4889201620150044>
- Conceição R.V., Green D.H. 2004. Derivation of potassic (shoshonitic) magmas by decompression melting of phlogopite+pargasite lherzolite. *Lithos*, 72(3-4):209-229. <https://doi.org/10.1016/j.lithos.2003.09.003>
- Davison I., Santos R.A. 1989. Tectonic evolution of the Sergipano fold belt, NE Brazil, during the Brasiliano Orogeny. *Precambrian Research*, 45(4):319-342. [https://doi.org/10.1016/0301-9268\(89\)90068-5](https://doi.org/10.1016/0301-9268(89)90068-5)
- D'el Rey Silva L.J. (1992). *Tectonic Evolution of the Southern Part of the Sergipano Fold Belt, Northeastern Brazil*. PhD Thesis, University of London, London, 288 p.
- Didier J. 1973. *Granites and their enclaves*. Amsterdam: Elsevier, 393 p.
- Dodge F.C.W., Kistler R.W. 1990. Some additional observations on inclusions in the granitic rocks of the Sierra Nevada. *Journal of Geophysical Research*, 95(B11):17841-17848. <https://doi.org/10.1029/JB095B11p17841>
- Elburg M.A. 1996. Evidence of isotopic equilibration between microgranitoid enclaves and host granodiorite, Warburton Granodiorite, Lachlan Fold Belt, Australia. *Lithos*, 38(1-2):1-22. [https://doi.org/10.1016/0024-4937\(96\)00003-5](https://doi.org/10.1016/0024-4937(96)00003-5)
- Elkins L.J., Gaetani G.A., Sims K.W.W. 2008. Partitioning of U and Th during garnet pyroxenite partial melting: Constraints on the source of alkaline ocean island basalts. *Earth and Planetary Science Letters*, 265(1-2):270-286. <https://doi.org/10.1016/j.epsl.2007.10.034>
- Fernandes D.M., Lisboa V.A.C., Rosa M.L.S., Conceição H. 2020. Petrologia e idade do Stock Fazenda Lagoas, Domínio Macururé, Sistema Orogênico Sergipano, NE-Brasil. *Geologia USP. Série Científica*, 20(1):39-60. <https://doi.org/10.11606/issn.2316-9095.v20-160040>
- Fernandez A.N., Barbarin B. 1991. Relative rheology of coeval mafic and felsic magmas: nature of resulting interaction processes and shape and mineral fabrics of mafic micro- granular enclaves. In: Didier J., Barbarin B. (Eds.). *Enclaves and granite petrology (developments in petrology)*. Amsterdam: Elsevier, p. 263-275.
- Foley S.F., Jackson S.E., Fryer B.J., Greenough J.D., Jenner G.A. 1996. Trace element partition coefficients for clinopyroxene and phlogopite

- in an alkaline lamprophyre from Newfoundland by LAM-ICP-MS. *Geochimica et Cosmochimica Acta*, **60**(4):629-638. [https://doi.org/10.1016/0016-7037\(95\)00422-x](https://doi.org/10.1016/0016-7037(95)00422-x)
- Foley S.F., Wheller G.E. 1990. Parallels in the origin of the geochemical signatures of island arc volcanics and continental potassic igneous rocks: The role of residual titanates. *Chemical Geology*, **85**(1-2):1-18. [https://doi.org/10.1016/0009-2541\(90\)90120-V](https://doi.org/10.1016/0009-2541(90)90120-V)
- Fontes M.P., Conceição H., Rosa M.L.S., Lisboa V.A.C. 2018. Minettes do Stock Monzonítico Glória Norte: evidência de magmatismo ultrapotássico pós-orogênico, com assinatura de subducção, no Sistema Orogrênico Sergipano. *Geologia USP. Série Científica*, **18**(1):51-66. <https://doi.org/10.11606/issn.2316-9095.v18-133599>
- Fourcade S., Allegre C.J. 1981. Trace elements behavior in granite genesis: a case study the calc-alkaline plutonic association from the Querigut Complex (Pyrenées, France). *Contributions to Mineralogy and Petrology*, **76**(2):177-195. <https://doi.org/10.1007/bf00371958>
- Frost B.R., Barnes C.G., Collins W.J., Arculus R.J., Ellis D.J., Frost C.D. 2001. A geochemical classification for granitic rocks. *Journal of Petrology*, **42**(11):2033-2048. <https://doi.org/10.1093/ptrology/42.11.2033>
- Frost B.R., Lindsley B.H. 1991. The occurrence of Fe-Ti oxides in igneous rocks. Oxide minerals: petrogenetic and magnetic significance. In: Lindsley B.H. (Ed.), *Oxide minerals: petrologic and magnetic significance*. Mineralogical Society of America, **25**, 433-486.
- Furman T., Graham D. 1999. Erosion of lithospheric mantle beneath the East African Rift system: geochemical evidence from the Kivu volcanic province. *Lithos*, **48**(1-4):237-262. [https://doi.org/10.1016/S0024-4937\(99\)00031-6](https://doi.org/10.1016/S0024-4937(99)00031-6)
- Gentil T. 2013. *Petrologia e Geoquímica do Batólito Shoshonítico Serra do Brejo no Domínio Poço Redondo, Faixa Sergipana (Sul da Província Borborema)*. MS Dissertation, Universidade Federal de Sergipe, Sergipe.
- Grégoire M., Moine B.N., O'Reilly S.Y., Cottin J.Y., Giret A. 2000. Trace element residence and partitioning in mantle xenoliths metasomatized by highly alkaline, silicate- and carbonate-rich melts (Kerguelen Islands, Indian Ocean). *Journal of Petrology*, **41**(4):477-509. <https://doi.org/10.1093/ptrology/41.4.477>
- Hall A. 1991. *Igneous Petrology*. Harlow: Longman Scientific & Technical.
- Hibbard M.J. 1991. Textural anatomy of twelve magma-mixed granitoid systems. In: Didier J., Barbarin B. (Eds.). *Enclaves and granite petrology (developments in petrology)*. Amsterdam: Elsevier, 431-444.
- Hollanda M.H.B.M., Pimentel M.M., Jardim de Sá E.F. 2003. Paleoproterozoic subduction-related metasomatic signatures in the lithospheric mantle beneath NE Brazil: inferences from trace element and Sr-Nd-Pb isotopic compositions of Neoproterozoic high-K igneous rocks. *Journal of South American Earth Sciences*, **15**(8):885-900. [https://doi.org/10.1016/S0895-9811\(03\)00014-2](https://doi.org/10.1016/S0895-9811(03)00014-2)
- Janoušek V., Braithwaite C.J.R., Bowes D.R., Gerdes A. 2004. Magma-mixing in the genesis of Hercynian calc-alkaline granitoids: an integrated petrographic and geochemical study of the Sázava intrusion, Central Bohemian Pluton, Czech Republic. *Lithos*, **78**(1-2):67-99. <https://doi.org/10.1016/j.lithos.2004.04.046>
- Kaczmarek M.A., Bodinier J.L., Bosch D., Tommasi A., Dautria J.M., Kechid S.A. 2016. Metasomatized mantle xenoliths as a record of lithospheric mantle evolution of the northern edge of the Ahaggar Swell, in Teria (Algeria). *Journal of Petrology*, **57**(2):345-382. <https://doi.org/10.1093/ptrology/egw009>
- Kepezhinskas P.K., Eriksen G.M.D., Kepezhinskas N.P. 2016. Geochemistry of ultramafic to mafic rocks in the Norwegian Lapland: inferences on mantle sources and implications for diamond exploration. *Earth Science Research*, **5**(2):148-187. <https://doi.org/10.5539/esrv.5n2p148>
- Krmiček L., Cempírek J., Havlín A., Přichystal A., Houzar S., Krmíčková M., Gadas P. 2011. Mineralogy and petrogenesis of a Ba-Ti-Zr-rich peralkaline dyke from Šebkovice (Czech Republic): Recognition of the most lamproitic Variscan intrusion. *Lithos*, **121**(1-4):74-86. <https://doi.org/10.1016/j.lithos.2010.10.005>
- Kumar S., Bora S., Sharma U.K., Yi K., Kim N. 2017. Early Cretaceous subvolcanic calc-alkaline granitoid magmatism in the Nubra-Shyok valley of the Shyok Suture Zone, Ladakh Himalaya, India: Evidence from geochemistry and U-Pb SHRIMP zircon geochronology. *Lithos*, **277**:33-50. <https://doi.org/10.1016/j.lithos.2016.11.019>
- Kumar S., Rino V. 2006. Mineralogy and geochemistry of microgranular enclaves in Palaeoproterozoic Malanjhand granitoids, central India: evidence of magma mixing, mingling, and chemical equilibration. *Contributions to Mineralogy and Petrology*, **152**:591-609. <https://doi.org/10.1007/s00410-006-0122-3>
- Kumar S., Rino V., Pal A. B. 2004. Field evidence of magma mixing from microgranular enclaves hosted in Palaeoproterozoic Malanjhand granitoids, central India. *Gondwana Research*, **7**(2):539-548. [https://doi.org/10.1016/S1342-937X\(05\)70804-2](https://doi.org/10.1016/S1342-937X(05)70804-2)
- Le Maître R.W., Bateman P., Dudek A., Keller J., Lameyre M., Le Bas M.J., Sabine P.A., Shimid R., Sørensen H., Streckeisen A., Wolley R., Zanettin B. 1989. *A classification of igneous rocks and glossary of terms*. Oxford: Blackwell Scientific Publications.
- Lima D. 2016. *Caracterização petrológica e geoquímica do Pluton Curitiba, Domínio Poço Redondo-Marancó, Cinturão Sergipano*. MS Dissertation, Universidade Federal de Pernambuco, Pernambuco.
- Lisboa V.A.C., Conceição H., Rosa M.L.S., Fernandes D.M. 2019. The onset of post-collisional magmatism in the Macururé Domain, Sergipano Orogenic System: The Glória Norte Stock. *Journal of South American Earth Sciences*, **89**:173-188. <https://doi.org/10.1016/j.jsames.2018.11.005>
- Liu L., Qiu J.S., Li Z. 2013. Origin of mafic microgranular enclaves (MMEs) and their host quartz monzonites from the Muchen pluton in Zhejiang Province, Southeast China: Implications for magma mixing and crust-mantle interaction. *Lithos*, **160-161**:145-163. <https://doi.org/10.1016/j.lithos.2012.12.005>
- Maniar P.D., Picolli P.M. 1989. Tectonic discrimination of granitoids. *Geological Society American*, **101**(5):635-643. [https://doi.org/10.1130/0016-7606\(1989\)101<0635:TDOG>2.3.CO;2](https://doi.org/10.1130/0016-7606(1989)101<0635:TDOG>2.3.CO;2)
- Middlemost E.A.K. 1985. *Magmas and magmatic rocks: an introduction to igneous petrology*. London and New York: Longman.
- Müller D., Groves D.I. 2019. *Potassic igneous rocks and associated gold-copper mineralization*. Springer International Publishing. <https://doi.org/10.1007/978-3-319-92979-8>
- Müller D., Rock N.M.S., Groves D.I. 1992. Geochemical discrimination between shoshonitic and potassic volcanic rocks from different tectonic settings: a pilot study. *Mineralogy and Petrology*, **46**:259-289. <https://doi.org/10.1007/BF01173568>
- Morrison G.W. 1980. Characteristics and tectonic setting of the shoshonite rock association. *Lithos*, **13**(1):97-108. [https://doi.org/10.1016/0024-4937\(80\)90067-5](https://doi.org/10.1016/0024-4937(80)90067-5)
- Nakamura N. 1974. Determination of REE, Ba, Fe, Mg, Na and K in carbonaceous and ordinary chondrites. *Geochimica et Cosmochimica Acta*, **38**(5):757-775. [https://doi.org/10.1016/0016-7037\(74\)90149-5](https://doi.org/10.1016/0016-7037(74)90149-5)
- Nardi L.V.S., Lima E.F. 2000. Hybridisation of mafic microgranular enclaves in the Lavras Granite Complex, southern Brazil. *Journal of South American Earth Sciences*, **13**(1-2):67-78. [https://doi.org/10.1016/S0895-9811\(00\)00006-7](https://doi.org/10.1016/S0895-9811(00)00006-7)
- Oliveira A.C. 2014. *Petrogênese do Stock Granítico Monte Alegre, noroeste do Domínio Macururé, Faixa Sergipana*. MS Dissertation, Universidade Federal de Sergipe, Sergipe.
- Oliveira E.P., Bueno J.F., McNaughton N.J., Silva Filho A.F., Nascimento R.S., Donatti-Filho J.P. 2015. Age, composition, and source of continental arc- and syn-collision granites of the neoproterozoic Sergipano belt, southern Borborema province, Brazil. *Journal of South American Earth Science*, **58**:257-280. <https://doi.org/10.1016/j.jsames.2014.08.003>
- Oliveira E.P., Toteu S.F., Araújo M.N.C., Carvalho M.J., Nascimento R.S., Bueno J.F., McNaughton N., Basili G. 2006. Geologic correlation between the Neoproterozoic Sergipano belt (NE Brazil) and the Yaoundé belt (Cameron, Africa). *Journal of African Earth Sciences*, **44**(4-5):470-478. <https://doi.org/10.1016/j.jafrearsci.2005.11.014>
- Oliveira E.P., Windley B.F., Araújo M.N.C. 2010. The Neoproterozoic Sergipano orogenic belt, NE Brazil: a complete plate tectonic cycle in western Gondwana. *Precambrian Research*, **181**(1-4):64-84. <https://doi.org/10.1016/j.precamres.2010.05.014>
- Pearce J.A. 1982. Trace element characteristics of lavas from destructive plate boundaries. In: Thorpe R.S. (Ed.). *Andesites: orogenic andesites and related rocks*. New York: Wiley, p. 525-548.

- Pearce J.A. 2008. Geochemical fingerprinting of oceanic basalts with applications to ophiolite classification and the search for Archean oceanic crust. *Lithos*, **100**(1-4):14-48. <https://doi.org/10.1016/j.lithos.2007.06.016>
- Peccerillo A., Taylor S.R. 1976. Geochemistry of Eocene calc-alkaline volcanic rocks from the Kastamonu area. *Contributions to Mineralogy and Petrology*, **58**:63-81. <https://doi.org/10.1007/BF00384745>
- Pereira F.S., Rosa M.L.S., Conceição H. 2019. Condições de colocação do magmatismo máfico do Domínio Macururé, Sistema Orogênico Sergipano: Maciço Capela. *Geologia USP. Série Científica*, **19**(3):3-29. <https://doi.org/10.11606/issn.2316-9095.v19-151464>
- Perugini D., Poli G. 2011. Intrusion of mafic magmas into felsic magma chambers: new insights from natural outcrops and fluid-mechanics experiments. *Italian Journal of Geosciences*, **130**(1):3-15. <https://doi.org/10.3301/IJG.2010.22>
- Perugini D., Poli G. 2012. The mixing of magmas in plutonic and volcanic environments: analogies and differences. *Lithos*, **153**:261-277. <https://doi.org/10.1016/j.lithos.2012.02.002>
- Perugini D., Poli G., Christofides G., Eleftheriadis G. 2003. Magma mixing in the Sithonia plutonic complex, Greece: evidence from mafic microgranular enclaves. *Mineralogy and Petrology*, **78**(3-4):173-200. <https://doi.org/10.1007/s00710-002-0225-0>
- Petford N. 2003. Rheology of granitic magmas during ascent and emplacement. *Annual Review of Earth and Planetary Sciences*, **31**:399-427. <https://doi.org/10.1146/annurev.earth.31.100901.141352>
- Pinho Neto M.A., Rosa M.L.S., Conceição H. 2019. Petrologia do Batólito Sítios Novos, Sistema Orogênico Sergipano, Província Borborema, NE do Brasil. *Geologia USP. Série Científica*, **19**(2):135-150. <https://doi.org/10.11606/issn.2316-9095.v19-152469>
- Reubi O., Blundy J. 2009. A dearth of intermediate melts at subduction zone volcanoes and the petrogenesis of arc andesites. *Nature*, **461**:1269-1273. <https://doi.org/10.1038/nature08510>
- Ringwood A.E. 1990. Slab-mantle interaction - Petrogenesis of intraplate magmas and structure of the upper mantle. *Chemical Geology*, **82**:187-207. [https://doi.org/10.1016/0009-2541\(90\)90081-H](https://doi.org/10.1016/0009-2541(90)90081-H)
- Rosa M.L.S., Conceição J.A., Lisboa V.A., Silva C.C., Pereira F.S., Conceição H. 2017. U-Pb Zircon Ages in Granites (940 to 583 Ma) in the Sergipano Orogenic System, NE Brazil. In: Goldschmidt 2017 (p. 3403-3403). Paris: Holanda: European Association of Geochemistry.
- Ruprecht P., Bergantz G.W., Cooper K.M., Hildreth W. 2012. The crustal magma storage system of Volcán Quizapu, Chile, and the effects of magma mixing on magma diversity. *Journal of Petrology*, **53**(4):801-840. <https://doi.org/10.1093/petrology/egs002>
- Ryan J.G., Morris J., Bebout G., Leeman B. 1996. Describing chemical fluxes in subduction zones: insights from "depth profiling" studies of arc and forearc rocks. In: Bebout G.E., Scholl D.W., Kirby S.H., Platt, J.P. (Eds.), *Subduction top to bottom* (p. 263-268). Washington, D.C.: American Geophysical Union.
- Santos I.S., Conceição H., Rosa M.L.S., Marinho M.M. 2019. Magmatismo shoshonítico e cálcio-alcálico de alto potássio pós-orogênico (615 Ma) na porção leste do Domínio Macururé, Sistema Orogênico Sergipano: Stocks Propriá, Amparo do São Francisco e Fazenda Alvorada. *Geologia USP. Série Científica*, **19**(1):99-116. <https://doi.org/10.11606/issn.2316-9095.v19-141362>
- Santos R.A., Martins A.A., Neves J.P., Leal R.A. 2001. *Programa Levantamentos Geológicos Básicos do Brasil - PLGB*. Geologia e recursos minerais do Estado de Sergipe. Escala 1:250.000. Texto Explicativo do Mapa Geológico do Estado de Sergipe. Brasília: CPRM/DIEDIG/DEPAT, CODISE.
- Santos R.A., Souza J.D. 1988. *Programa Levantamentos Geológicos Básicos do Brasil*. Carta Geológica Piranhas. Escala 1:100.000. Brasília: DNPM/CPRM.
- Sarjoughian F., Lentz D., Kananian A., Ao S., Xiao W. 2017. Geochemical and isotopic constraints on the role of juvenile crust and magma mixing in the UDMA magmatism, Iran: evidence from mafic microgranular enclaves and cogenetic granitoids in the Zafarghand igneous complex. *International Journal of Earth Sciences*, **107**(3):1127-1151. <https://doi.org/10.1007/s00531-017-1548-8>
- Shukla S., Mohan M.R. 2019. Magma mixing in Neoproterozoic granite from Nalgonda region, Eastern Dharwar Craton, India: Morphological, mineralogical and geochemical evidences. *Journal of Earth System Science*, **128**(3):71. <https://doi.org/10.1007/s12040-019-1095-8>
- Silva C.C. 2014. *Petrologia e geocronologia do Stock Granodiorítico Lagoa do Roçado, Domínio Macururé, Faixa Sergipana-SE*. MS Dissertation, Universidade Federal de Sergipe, Sergipe.
- Silva Filho M.A., Torres H.H. 2002. A new interpretation on the Sergipano Belt domains. *Anais da Academia Brasileira de Ciências*, **74**(3):556-557. <https://doi.org/10.1590/S0001-37652002000300049>
- Siuda J.D., Bagiński B. 2019. Magma mingling textures in granitic rocks of the eastern part of the Strzegom-Sobótka Massif (Polish Sudetes). *Acta Geologica Polonica*, **69**(1):143-160. <https://doi.org/10.24425/agp.2019.126437>
- Smith E.I., Sánchez A., Walker J.D., Wang K. 1999. Geochemistry of Mafic Magmas in the Hurricane Volcanic Field, Utah: Implications for Small- and Large-Scale Chemical Variability of the Lithospheric Mantle. *The Journal of Geology*, **107**(4):433-448. <https://doi.org/10.1086/314355>
- Sousa C.S., Soares H.S., Rosa M.L.S., Conceição H. 2019. Petrologia e Geocronologia do Batólito Rio Jacaré, Domínio Poço Redondo, Sistema Orogênico Sergipano, NE do Brasil. *Geologia USP. Série Científica*, **19**(2):171-194. <https://doi.org/10.11606/issn.2316-9095.v19-152494>
- Streckeisen A. 1976. To each plutonic rock its proper name. *Earth Science Reviews*, **12**(1):1-33. [https://doi.org/10.1016/0012-8252\(76\)90052-0](https://doi.org/10.1016/0012-8252(76)90052-0)
- Sun S.S., McDonough W.F. 1989. Chemical and isotopic systematics of oceanic basalts: implications for mantle composition and processes. *Geological Society, London, Special Publications*, **42**(1):313-345.
- Thompson R.N. 1982. Magmatism of the British Tertiary Volcanic Province. *Scottish Journal of Geology*, **18**:49-107. <https://doi.org/10.1144/sjg18010049>
- Torkian A., Furman T. 2015. The significance of mafic microgranular enclaves in the petrogenesis of the Qorveh Granitoid Complex, northern Sanandaj-Sirjan Zone, Iran. *Neues Jahrbuch Für Mineralogie – Abhandlungen. Journal of Mineralogy and Geochemistry*, **192**(2):117-133. <https://doi.org/10.1127/njma/2015/0275>
- Turner S., Arnaud N., Liu J., Rogers N., Hawkesworth C., Harris N., Kelley S., Van Calsteren P., Deng W. 1996. Post-collision, Shoshonitic Volcanism on the Tibetan Plateau: Implications for Convective Thinning of the Lithosphere and the Source of Ocean Island Basalts. *Journal of Petrology*, **37**(1):45-71. <https://doi.org/10.1093/petrology/37.1.45>
- Vernon R.H. 1984. Microgranitoid enclaves in granites: globules of hybrid magma quenched in a plutonic environment. *Nature*, **309**:438-439. <https://doi.org/10.1038/309438a0>
- Vernon R.H., Etheridge M.A., Wall V.J. 1988. Shape and microstructure of microgranitoid enclaves: indicators of magma mingling and flow. *Lithos*, **22**(1):1-11. [https://doi.org/10.1016/0024-4937\(88\)90024-2](https://doi.org/10.1016/0024-4937(88)90024-2)
- Weidendorfer D., Mattson H.B., Ulmer P. 2014. Dynamics of magma mixing in partially crystallized magma chambers: textural and petrological constraints from the Basal Complex of the Austurhorn Intrusion (SE Iceland). *Journal of Petrology*, **55**(9):1865-1903. <https://doi.org/10.1093/petrology/egu044>
- Winter J.D. 2014. *Principles of Igneous and Metamorphic Petrology* (2^a ed.). Edinburgh: Pearson New International Edition.
- Wones D.R. 1989. Significance of the assemblage titanite + magnetite + quartz in granitic rocks. *American Mineralogist*, **74**(7-8):744-749.
- Wyllie P.J., Cox K.G., Biggar G.M. 1962. The Habit of Apatite in Synthetic Systems and Igneous Rocks. *Journal of Petrology*, **3**(2):238-243. <https://doi.org/10.1093/petrology/3.2.238>
- Yang H., Ge W., Zhao G., Dong Y., Xu W., Ji Z., Yu J. 2015. Late Triassic intrusive complex in the Jidong region, Jiamusi-Khanka Block, NE China: Geochemistry, zircon U-Pb ages, Lu-Hf isotopes, and implications for magma mingling and mixing. *Lithos*, **224-225**:143-159. <https://doi.org/10.1016/j.lithos.2015.03.001>
- Zack T., Foley S.F., Jenner G.A. 1997. A consistent partition coefficient set for clinopyroxene, amphibole and garnet from laser ablation microprobe analysis of garnet pyroxenites from Kakanui, New Zealand. *Neues Jahrbuch für Mineralogie, Abhrichten*, **172**(1):23-41. <https://doi.org/10.1127/njma/172/1997/23>